METAL NANO-STRUCTURES FOR CATALYTIC APPLICATIONS WITH CHARACTERIZATION OF BEHAVIOR UNDER REACTION CONDITIONS

By

ANDISHAEH DADGAR

Bachelor of Science in Chemical Engineering

Oklahoma State University

Stillwater, Ok

2016

Submitted to the Faculty of the
Graduate College of the
Oklahoma State University
in partial fulfillment of
the requirements for
the Degree of
MASTER OF SCIENCE
August 2018

METAL NANO-STRUCTURES FOR CATALYTIC APPLICATIONS WITH CHARACTERIZATION OF BEHAVIOR UNDER REACTION CONDITIONS

Thesis Approved:

Dr. Marimuthu Andiappan

Thesis Advisor

Dr. Jindal Shah

Dr. Kalkan Kaan

Dr. Josh Ramsey

ACKNOWLEDGEMENTS

I would like to thank my adviser Dr. Marimuthu Andiappan for all of his help throughout this work and my master's degree.

To Farshid and Ravi, thank you for all of your friendship and help throughout my time with you. I appreciate our time more than I have shown.

I would like to also acknowledge my committee for all of the help along the way with this work as well as professional development and advice they have given me.

I would like to thank the core facility support staff, Dr. Steve Hartson for help with ESI-MS and HPLC, Lisa and Brent for help with the countless TEM and SEM samples over the last 2 years. I could not have made the progress I have without their time and dedication.

To Logan and Britten, thank you for all of your work in the lab making catalyst and running reactions. You helped me greatly.

I would like to say thank you to my fiancé Natalie for all of her help along the way and keeping my spirits up.

Finally, I would like to thank my parents Ali and Billie Dadgar for all of their help through my undergraduate and graduate schooling. Without their help I would not be able to be where I am today.

Acknowledgements reflect the views of the author and are not endorsed by committee members or Oklahoma State University.

Name: ANDISHAEH DADGAR

Date of Degree: AUGUST 2018

Title of Study: METAL NANO-STRUCTURES FOR CATALYTIC APPLICATIONS WITH CHARACTERIZATION OF BEHAVIOR UNDER REACTION CONDITIONS

Major Field: CHEMICAL ENGINEERING

Abstract:

Metal nanostructures are being used for more applications than ever before. Greater understanding of these structures for use in catalysis as well as energy transfer for bimetallic catalyst needs greater focus to drive rational design for future processes. By combining finite difference time domain simulations (FDTD) with experimental techniques, understanding of well-defined metal nanostructures may be gained under relevant conditions such as synthesis and reactions. In order to characterize these metal nanostructures under relevant conditions, Sonogashira coupling has been chosen to serve as a model reaction system with Au and Cu nanoparticles used as catalyst. Experimental results were found to closely correlate with FDTD simulation results for both growth of Au nanostructures and leaching under reaction conditions. CID(Chemical Interface Damping) is the primary energy transfer mechanism in Cu_2O/Cu structures but DET(Direct Electron Transfer) and RET(Resonant Energy Transfer) are still possible. In Sonogashira coupling, copper nanoparticles were found to act as a precursor for homogenous catalyst in the presence of base. Without base, the particles were found to be stable with the reaction proceeding heterogeneously on the surface of copper nanoparticles. FDTD simulations were correlated with known imaging techniques and experimental data, therefore a quick effective tool has been developed to determine particle size and shape without using electron microscopy or x-ray techniques. By understanding CID to be the dominate transfer mechanism in bimetallic structures, future bimetallic structures can be designed to harness light more effectively. Rational design can now be applied for future structures with tunable energy transfer. Finally, Sonogashira coupling can be performed without the addition of base, palladium, or phosphine ligands. This opens the possibility to improve other cross coupling reactions with heterogeneous nanoparticle catalyst.

TABLE OF CONTENTS

Chapter Page

I. INTRODUCTION 1

FDTD Modeling of Nanoparticles and Nanoalloys 1
Control of Oxide Thickness on Cu_2O/Cu via Partial Reduction 2
Copper based Ligand and Palladium Free Sonogashira Coupling 4
Scope of Thesis 5

II. REVIEW OF LITERATURE 7

Localized Surface Plasmon Resonance Spectroscopy 7
Surface Plasmon Resonance 11
Sonogashira Coupling 15

III. METHODOLOGY 21

FDTD Simulations 21
Copper Catalyst Preparation 21
Analytical Measurements 22
Reaction Procedures 24

Chapter Page

IV. FINDINGS 25

LSPR Spectroscopy as a Platform for Nanoparticle Stability by Utilizing FDTD Simulations 25
Determination of Energy Transfer Pathways in Cu2O/Cu Nanostructures 31
Copper based Ligand and Palladium Free Sonogashira Coupling 38

V. CONCLUSION 47

Modeling of Nanoparticles and Nanoalloys 47
Control of Oxide Thickness on Cu_2O/Cu via Partial Reduction 47
Copper based Ligand and Palladium Free Sonogashira Coupling 48

REFERENCES 50

APPENDICES 58

LIST OF TABLES

Table Page

Table 1 42

LIST OF FIGURES

Figure Page

1.2 4
1.3 5
2.1.1 8
2.1.2 8
2.1.3 10
2.1.4 10
2.2.1 12
2.2.2 13
2.2.3 14
2.3.1 15
2.3.2 17
2.3.3 18
2.3.4 19
4.1.1 26
4.1.2 27
4.1.3 29
4.1.4 30
4.2.1 32
4.2.2 33
4.2.3 35
4.2.4 36
4.3.1 37
4.3.2 39
4.3.3 41
4.3.4 43
4.3.5 44
4.3.6 45
A1a....59
A1b....60
A2a....60
A2b....61
A3....61
A4....62
A5....62
A6....63
A7....63
A8....64
A9....64
A10....65

Figure Page
A11....65
A12....66
A13....66
A14....67
A15....67
A16....68
A17....68
A18....70
A19....70
A20....71
A21....71
A22....71

CHAPTER I

Introduction

1.1 Modeling of Nanoparticles and Nanoalloys

Coupling reactions represent a large class of reactions and are estimated to be one out of every four reactions carried out in pharmaceutical processes.[1] These reactions have been traditionally carried out by homogeneous palladium (Pd) complexed catalyst.[1] Pd metal and most of the ligands associated with the homogeneous catalyst are toxic ;therefore the traditional homogeneous Pd-catalyzed processes generally require number of expensive downstream unit operations to reduce the metal content below the acceptable level in the active pharmaceutical ingredient (API).[2–4] In recent years, heterogeneous metal nanocatalysts have emerged as valuable alternatives to traditional homogenous complexes to drive coupling reactions. For example, nanocatalysts built on palladium (Pd), gold (Au), copper (Cu) and their alloys can drive coupling reactions at mild reaction temperatures, exhibit excellent yield, catalytic activity, and broad substrate scope.[5–7] These catalysts do not require ligands and are in general not sensitive to air and moisture. They therefore have the potential to avoid or reduce the need for the expensive downstream operations for separating the metal catalyst from the final product (e.g., API).

While nanoparticle uses has increased, determination of stability under relevant reaction conditions and identification of catalytic pathways remain ongoing challenges within the field. A common leaching test used to determine stability of nanocatalyst employs a filtration test. This test involves the analysis of the leached metal atoms in the filtered supernatant reaction solution

using techniques such as ICP-MS, and/or characterization (e.g., activity test) of the filtered solid catalyst. [8–11] This test has several drawbacks; for example, it has been reported that the leached metal atom can redeposit quickly back onto the catalyst during filtration and may not be detected in the supernatant solution.[8,10,12,13]

Herein, for cross coupling reactions involving metal nanoparticles such as copper, gold, palladium, we propose an alternate and novel method that is based on their interesting optical properties of these metals. These metals at a nanoscale exhibit localized surface plasmon resonance (LSPR), which can be monitored through UV-Vis spectroscopy. By measuring the extinction spectra of the nanoparticles, which is defined as scattered and absorbed light, insights can be gained as the LSPR response can be directly correlated to size of plasmonic metal nanoparticles.

1.2 Control of Oxide Thickness on Cu_2O/Cu via Partial Reduction

Synthesis of nanostructures has rocketed to the forefront of inorganic synthetic procedure development within the last twenty years. These procedures range from total inert conditions with moisture control to open air with simple stirring. For air sensitive procedures, like that of copper prepared by micro-emulsion techniques the presence of air, specifically oxygen, leads to an undesirable formation of metal oxide on the surface of the particles. Within the field of heterogeneous metal catalysis, this issue has been addressed for many years as the active form of most metal catalyst being the pure form not the oxide. [14] Copper in particular is known in the presence of excess oxygen and heat to rapidly oxidize to Cu_2O or CuO depending on the conditions.[15] In the field of plasmonic catalysis though this shell, a semi-conductor, changes the energy distribution of the surface plasmons within the core.[16–18] The change in energy transfer is noticed in the UV-Vis extinction spectra of the particles at 550 nm, or the surface plasmon peak for copper nanoparticles. As opposed to other coatings on the surface of plasmonic particles, i.e.

capping agents and organic stabilizers, this oxide coating offers a conductive media to transfer the surface plasmon energy via multiple different pathways. The first pathway is chemical interface damping (CID). This mechanism involves the direct transfer of plasmon energy into overlapping unpopulated states of the oxide coating as seen in Fig 1.3.a.[19–22] The second pathway is by absorbed plasmonic energy transferred after thermalization via DET.[19] When plasmons follow damping and thermalization the energy level of the plasmon distribution is much closer to that of the fermi level of the metal as seen in Fig 1.3.b.[9,23–25] As well, energy can transfer through resonance, more aptly named resonate energy transfer (RET).[20] In this process the energy given off by the core couples with the shell valence band and upon decay of the surface plasmon an energetic electron is excited to the conduction band with a hole being left in the core material. The mechanism of each pathway is vastly different but distinguishing between them has large implications within the field of bimetallic nanostructures. For instance, if CID is responsible for energy transfer between two structures then only the energy overlapping with unfilled states will be transferred while in RET and DET e/h pairs are excited to discrete positions within the adsorbate valance structure. Distinguishing between CID, DET, and RET is critical for the design of efficient solar cells, water splitting bimetallic structures as well as sensing devices to name a few mechanistic design cases.[26–29]

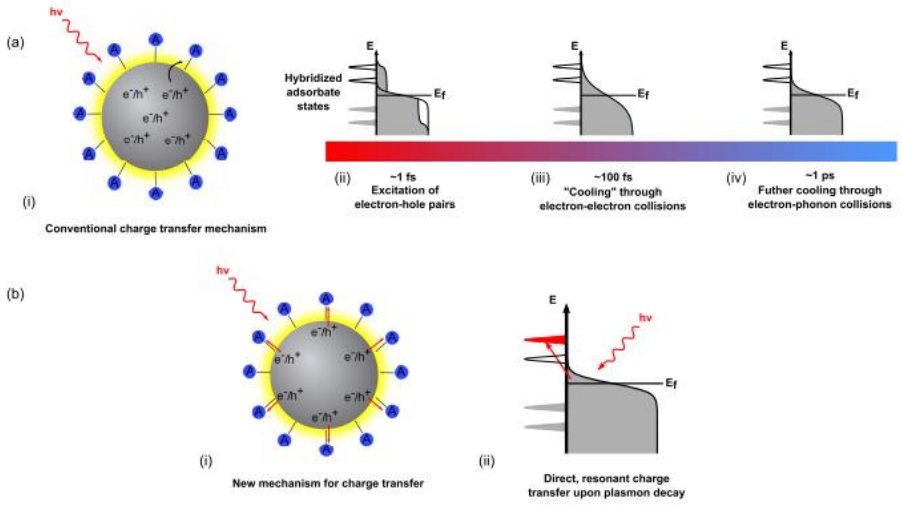

Figure 1.2 Charge transfer and plasmon decay modes within plasmonic nanoparticles excited by incident light. Pathway a.) represents Landau damping and thermalization of SPR generated energy. Pathway b.) follows direct transfer of SPR energy to adsorbed chemicals (CID). From Boerigter et al. [30]

To help distinguish between the mechanisms, Cu_2O/Cu is studied here due to the ease of preparation and stability for analysis. By preparing the particles in an air rich environment, a thin shell of oxide will be formed on the copper cores. Then this shell may be removed by heating under the flow of hydrogen gas thereby reducing the oxide to water vapor. Controlling the time at temperature and hydrogen exposure then affords control of the oxide thickness. In controlling thickness, a deeper understanding may be found about the energy transfer mechanisms between surface plasmon energy and conductive nonplasmonic materials, such as semiconductors, because as the shell thickness decreases energy flow to the shell thickness will change accompanied by spectral changes for the LSPR. Using LSPR spectroscopy, diffuse reflectance spectroscopy, XRD, and FDTD simulations, changes in surface interactions between Cu_2O/Cu can be monitored such that the dominate charge transfer mechanism may be determined.

1.3 Copper based Ligand and Ligand Free Sonogashira Coupling

C-C bond formation remains one of the most widely used classes of organic synthesis reactions today.[31–33] Within our growing world, a greater demand has been placed on organic protocols to reduce cost while increasing productivity with lower waste generation. Within C-C

bond forming reactions, cross couplings stand out as a gold standard of synthetic protocols. These reactions cover a wide range of C-C bonding under many different conditions. One family of cross coupling reactions, known as Sonogashira coupling, is frequently used to insert a triple bond in between two aryl groups.

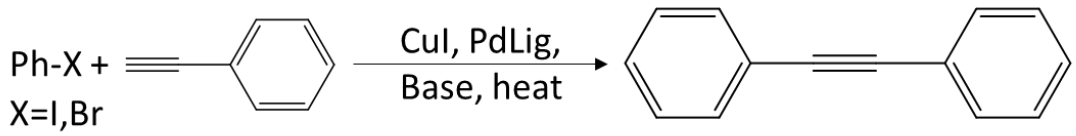

Figure 1.3 Schematic showing typical Sonogashira coupling conditions

The reaction protocol calls for homogenous palladium catalyst with a homogenous copper co-catalyst. Since the palladium catalyst are typically air sensitive, inert environments are need to maintain the catalyst for the entire reaction. As well, the palladium blacks out at the end of the reaction commonly, depositing pallidum black in the reactor that must be adsorbed and removed before the next batch. This means that fresh copper and palladium must be added to each batch. With demand increasing and budgets decreasing, a new breakthrough is needed to move Sonogashira coupling toward the future. Many efforts to do so have focused on using less copper, less palladium, and less ligand loadings.[34–36] While these are all valid ways of decreasing overall cost, they do nothing to increase production or significantly reduce costs. To reduce the cost drastically, we propose to remove palladium and ligands all together and use only copper nanoparticles as the primary catalyst. To use copper itself as the primary catalyst is not a new concept but using only copper nanoparticles suspended in solution is completely novel.[37,38] This will completely eliminate the need for costly palladium catalyst as well as toxic, expensive phosphorus ligands. These nanoparticles have another major advantage as discussed previously in that copper nanoparticles and copper complexes interact with visible light. By shining visible light corresponding to the SPR peak of copper, reaction rates may be increased with lower temperatures allowing for additional cost savings from energy input. Copper nanoparticles as we

will show in this work, represent a new direction in Sonogashira coupling that will be able to meet the demands of a growing world.

1.4 Scope of Thesis

This thesis primarily focuses on noble metal nanoparticles of copper, gold, and silver and how their properties may be used for relevant catalytic processes. The goals then are 1.) simulate and correlate Cu, Au, Ag, and bimetallic Pd/Ag nanoparticles to help correlate UV-Vis findings with noble metal nanoparticle stability leading to mechanistic understanding 2.) investigate energy transfer mechanisms primarily chemical interface damping (CID), direct electron transfer (DET), and resonant energy transfer (RET) within copper nanoparticles with cuprous oxide coatings for a better understanding of bimetallic structures and 3.) use copper nanoparticles to improve catalytic C-C bond formation within organic synthesis protocols with a focus on Sonogashira coupling of phenylacetylene and iodoaryls.

CHAPTER II

Review of Literature

2.1 Localized Surface Plasmon Resonance Spectroscopy

By using the surface plasmon excitation discussed previously, a whole field of spectroscopy is possible now. The use of plasmonic particles to enhance detection, response, or as a detector itself has been given the name surface plasmon resonance (SPR) spectroscopy. When these techniques are applied using single nanoparticles and not a deposited surface then it is called localized surface plasmon spectroscopy or LSPR spectroscopy. Within LSPR spectroscopy, there are common techniques that call for further discussion.

First is surface enhanced Raman spectroscopy (SERS). The first use of this technique was reported in 1973 by Fleischmann et al.[39] Since then there have been countless uses for this technique from biological assays to traditional catalytic studies. Traditional Raman spectroscopy uses the excitation and decay of energetic bonds within vibrational states of molecules to detect functional groups and structure.[40] The detection of inelastic scattering then is reported as excited vibrational modes decay to a wavelength not of the incident light as in other forms of spectroscopy. This decay though is not as common as nonradiative emission so detection limits are high. By incorporating silver nanostructures into the system, Fleishmann et al. were able to greatly increase the photon density near the surfaces of interest by orders of 10^{11}. This allows for detection of single molecule adsorption onto a metal surface.[41] To improve detector response, thin films with raised plasmonic substrates have been used to increase the scattering effect of the

silver particles. These films use a deposition/etching technique to create raised pyramidal structures which allow for even further intensified light due to the sharp corners and proximity to each other. [42] More recently, it has been shown by Willets et al. that by attaching receptors onto the surface of silver particles biological assays can be performed to femtomolar concentrations very accurately. With such low detection capabilities, the application of SERS is certain to leave a mark on the field of plasmonics.

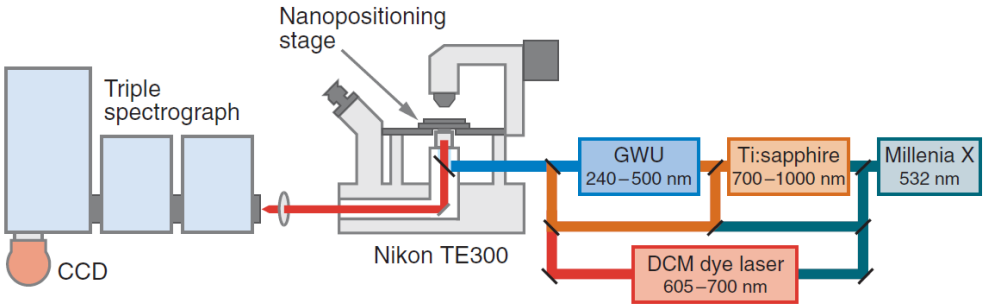

Figure 2.1.1 Typical SERS set up with additional laser wavelength options for enhanced detection capabilities from Willets et al.[42]

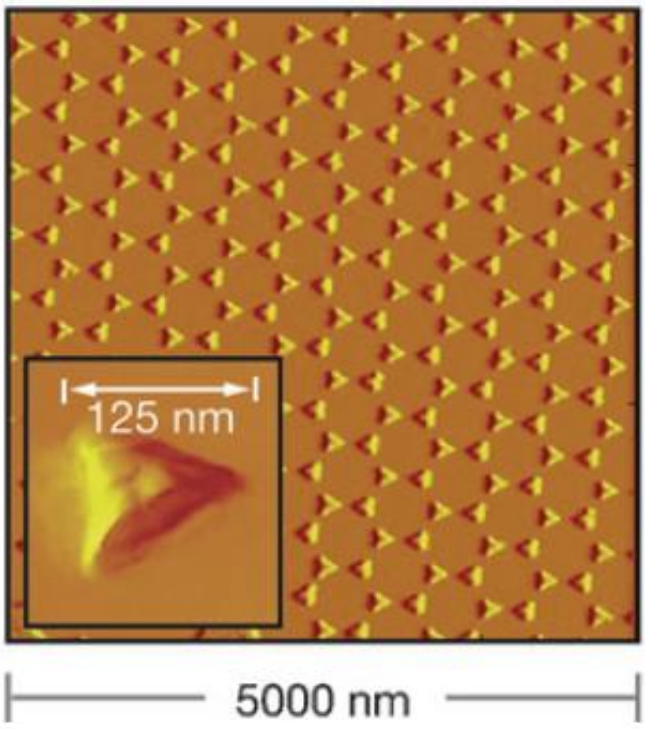

Figure 2.1.2 Atomic force mapping image of silver pyramid structures on an inert substrate for SERS from Willlets et al[42]

Futhermore, UV-Vis spectroscopy can be classified as LSPR spectroscopy when dealing with suspended or supported plasmonic metal nanoparticles. UV-Vis spectroscopy is able to give the extinction spectra of nanoparticles which can be of great interest. For plasmonic nanoparticles the extinction spectrum is closely tied to particle size, shape, and local environment around the particle.[43] The coupling of physical properties with the extinction spectra of the particle is due to the nature of the surface plasmon excitation. During the excitation the surface cloud of electrons is excited by an incoming electromagnetic field. As the surface facets and size of the particle change the response of the particles in UV-Vis spectra will change. For instance, for silver cubes of increasing size the LSPR peak shifts away from 450 nm up to 520 nm.[44] This shift is easily quantified using LSPR spectroscopy of Ag cubes in solution. As well, the peak width in the extinction spectra is directly correlated to the dispersity of plasmonic nanoparticles in solution. It was shown by Amendola et al. that by using Mie theory the average size of Au spheres and spheroids can be readily determined from just UV-Vis spectra.[45] These results were validated against electron microscopy images with deviations of 6% on average. As well as particle size distribution, energy flow in bimetallic or contacting metal nanoparticles can be determined. For instance, in composites of Au/TiO2 the UV-Vis spectra is able to see the transfer of energy from the surface plasmon excitation of gold. This transfer manifests as a decrease in the response of the LSPR from what is expected at the same size alone.[46] By examining the way the spectra change the energy transfer pathway can be determined using just the extinction spectra.

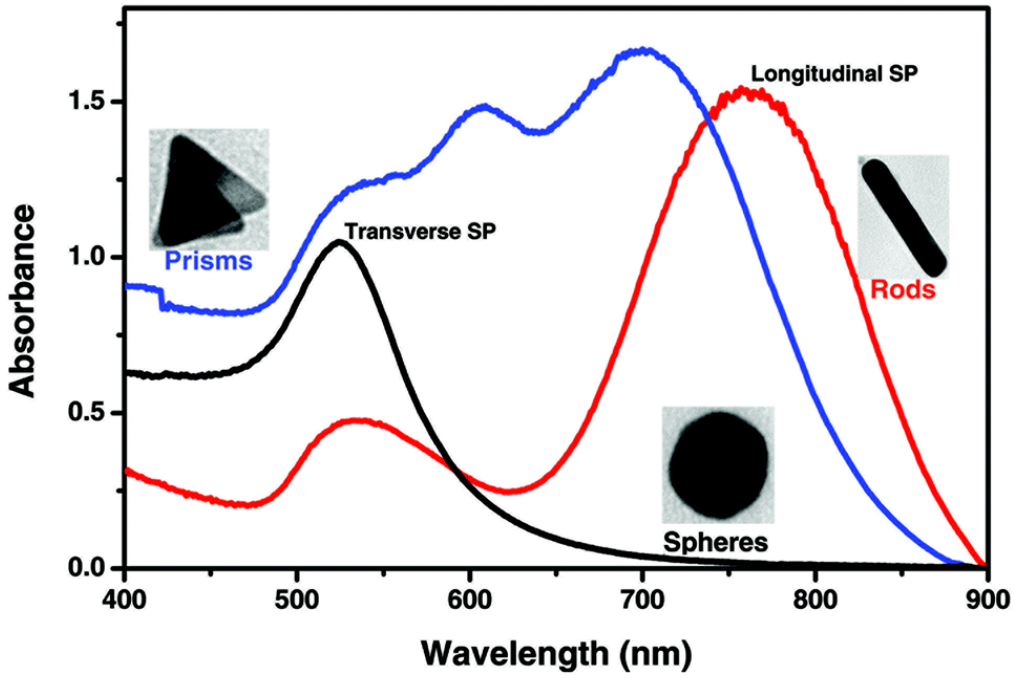

Figure 2.1.3 Representative extinction spectra for silver nanoparticles of various sizes and shapes. From Attia et al[47]

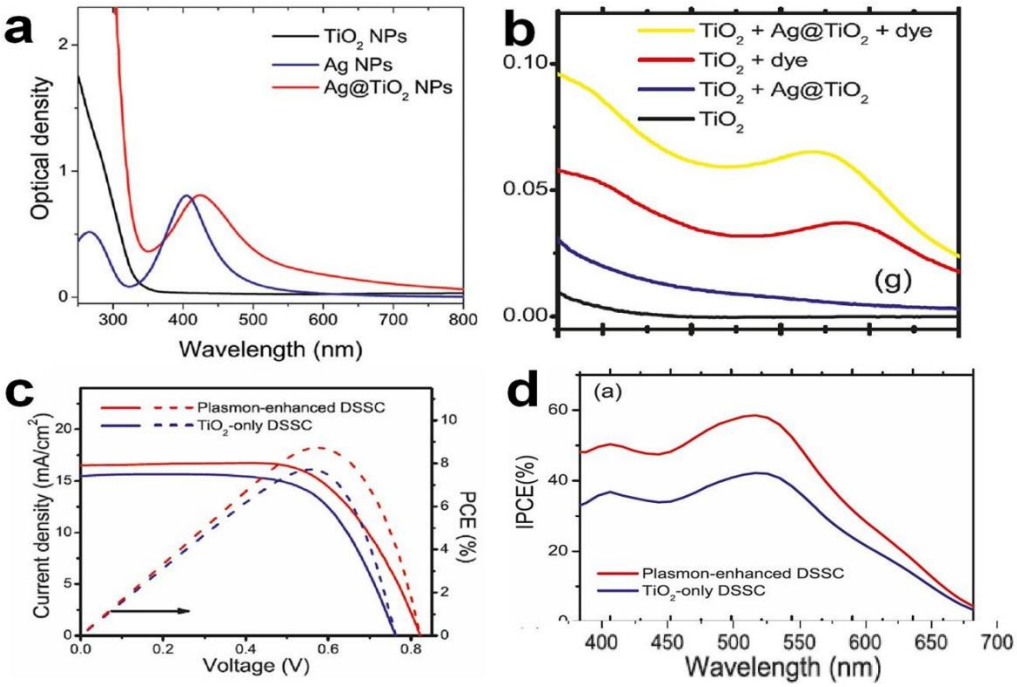

Figure 2.1.4 Extinction spectra for silver nanoparticles, TiO_2 nanoparticles, and Ag-TiO_2 nanostructures showing energy transfer from silver to TiO_2. From Ma et al.[46]

These two techniques are the most commonly used LSPR spectroscopic techniques. Both of these techniques offer powerful insights into a host of issues. For SERS, the advancements in single molecule adsorption as well as detection of biological agents at ultralow quantities has allowed for identification of reaction intermediates, unknown receptor interactions, and quantification of ultralow concentration biological molecules.[48–50] LSPR spectroscopy using UV-Vis is just as powerful of a tool for plasmonic nanoparticles. UV-Vis can be used to determine size, shape, dispersity, and energy transfer pathways all with a noninvasive or destructive technique. As well with simple correlations, LSPR spectroscopy can be used to replace costly electron imaging and dynamic light scattering measurements used to find average particle size and shapes.

2.2 Surface Plasmon Resonance

Incoming electromagnetic radiation can interact with metal nanoparticles of sizes much smaller than the wavelength. This interaction can cause a collective oscillation of free conduction band electrons on the metal surface. It is these oscillations that we know as surface plasmon excitation. The oscillations occur when the excitation due to incident electromagnetic radiation are restored by forces from the nuclei of the surface atoms. When this oscillation matches the wavelength of the incident radiation constructive interference occurs and the oscillation is magnified; this is said to be the resonance point for the system. The frequency and wavelength that this occurs at is known as the surface plasmon resonance (SPR). The resonant frequency depends then on the metal, particle shape, particle size, and dielectric media around the system.[43] For transition metals, copper, gold, and silver nanostructures have a free electron density and restorative force that lead to resonance in the visible region of light.

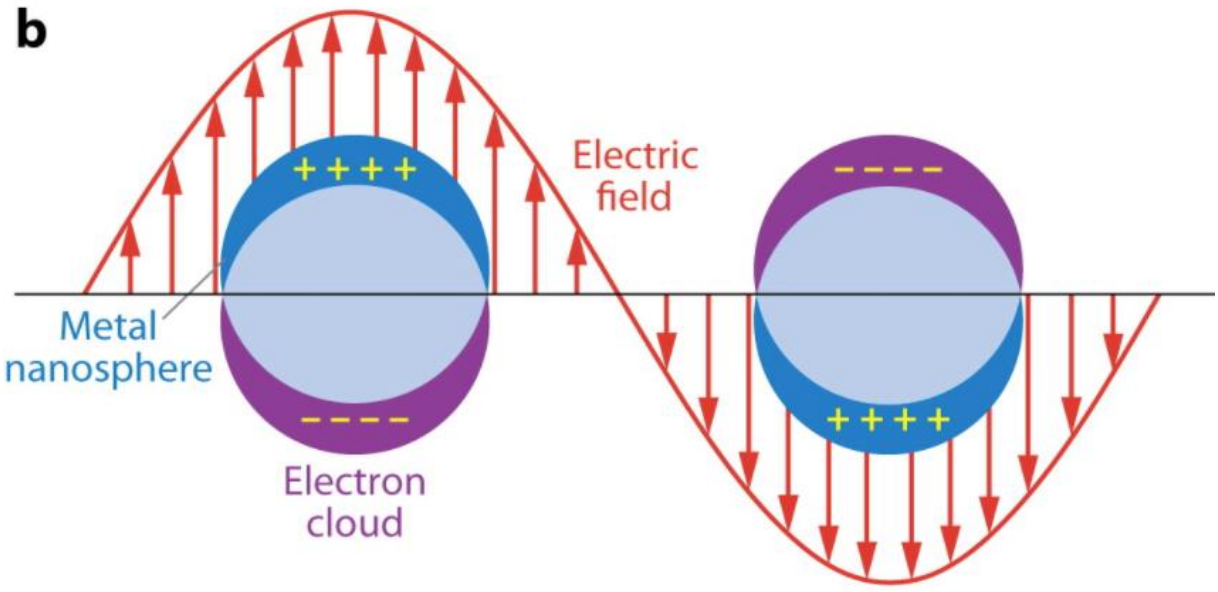

Figure 2.2.1 Collective excitation of the electron cloud of spherical metal nanoparticles by an electromagnetic field from Lu et al.[51]

Surface plasmon energy can be treated as a collective excitation of electrons above the fermi level of the bulk metal. This energy may be determined by using UV-Vis spectroscopy. During UV-Vis spectroscopy the incident light used for sensing of absorption is able to interact with the nanostructures and excite the surface plasmon. The spectrophotometer then interprets this interaction across the UV to visible region of light. When the particles resonate, the maximum peak position and extinction value can be determined from the spectra. The energy determined from UV-Vis spectroscopy is the total light energy that goes into the excitation of the surface plasmon that is scattered light and absorbed light.

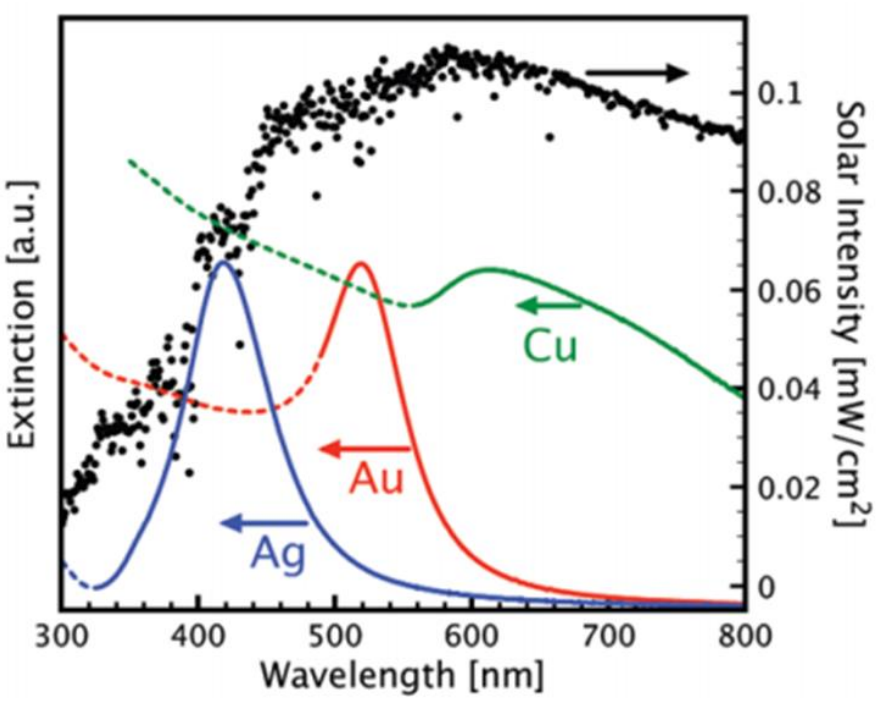

Figure 2.2.2 Simulated extinction spectra for Ag, Au, and Cu with the measured solar spectrum adapted from Linic et al.[52]

Once the surface plasmon has been excited, the plasmon can decay in several ways. The first way is by intense non-radiative scattering of light at the same wavelength as the SPR. The second way is by Landau damping or generation of energetic electrons within the bulk metal ultimately dissipating the energy into the vibrational modes of the bulk structure (i.e. heating). Each mode contributes differently to the overall extinction of the particle depending on size and shape of the metal nanoparticle. For instance, at smaller sizes, less than 10 nm, Landau damping dominates the extinction; while for larger sizes, greater than 100 nm scattering of the incident light contributes most to the extinction.

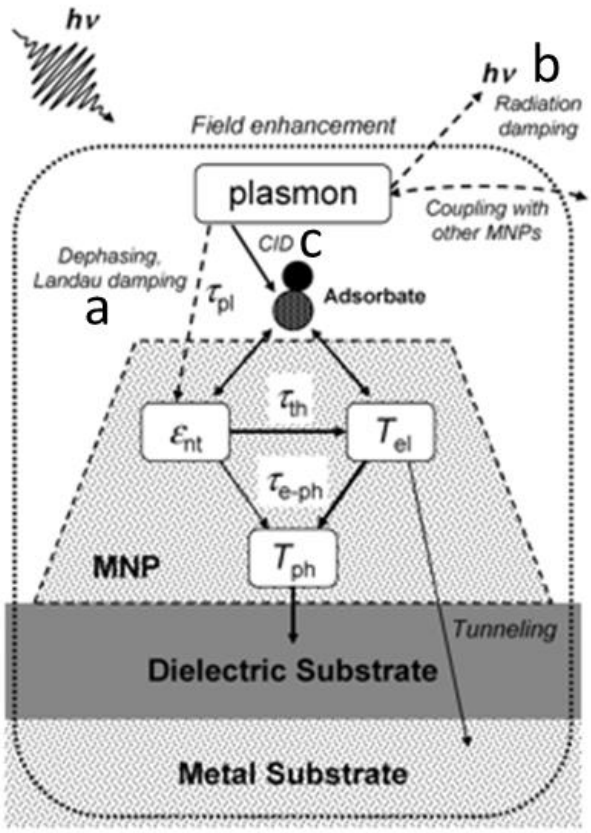

Figure 2.2.3 a.) Landau damping of excited plasmon states into the bulk of a metal nanoparticle. B.) scattering of plasmon energy through non-radiative scattering c.) transfer through CID of plasmon energy to adsorbates on the surface of a metal nanoparticle adapted from Watanbe et al.[53]

When the light is scattered back after plasmon excitation the electromagnetic field is highly concentrated near the surface. This leads to great enhancements of light flux and intensity near the surface of the nanoparticle as opposed to the incident light.[52] The enhancement of light flux near the surface can then be used to drive other photochemical processes such as dye oxidation or water splitting.[54,55] When chemical species are absorbed onto the surface, they can interact directly with the excited electron distribution. This interaction is known as chemical interface damping (CID). Through CID, the energy from the plasmon excitation is transferred directly into unpopulated adsorbate states at the same level as the plasmon states. It has been shown that through CID and indirectly through Landau damping the energy harvested from the incident light can be used to perform photochemical transformations and drive chemical reactions using light.[55]

Through excitation of the conduction band electrons by incident electromagnetic waves, surface plasmon resonance in Cu, Ag, and Au nanostructures provides an exciting field of study. Structures of these metals can be found in optics, medical sensing, imaging, and high resolution spectroscopic techniques. The optical properties of these particles along with the ability to enhance fields close to the surface certainly make plasmonic nanostructures a valuable asset for the future.

2.3 Sonogashira Coupling

Within organic chemistry, cross coupling reactions are the premier way of making C-C bonds between a variety of molecules.[56] For joining of two aryl group with a triple bond in between there are two paths that can be taken such as double elimination of bromine, and Sonogashira coupling. Sonogashira coupling involves the coupling of terminal alkynes with aryl halides. This preserves the triple bond between the two substrates with no need for protecting groups and harsh conditions.

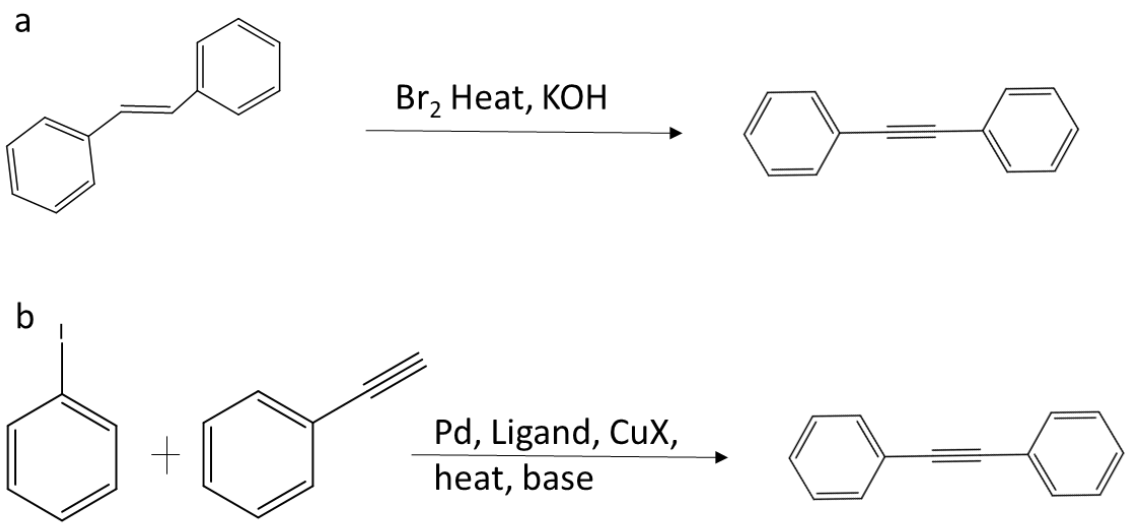

Figure 2.3.1 a.) Double elimination of bromine from trans stilbene to produce diphenylactylene b.) Sonogashira coupling of iodobenzene with phenylacetylene to produce diphenylactylene X=I,Br

Sonogashira coupling was first reported in 1975 as a way to perform alkyne insertions at low temperatures. The original protocol calls for a homogenous palladium catalyst with a catalytic amount of copper iodide as a co catalyst in an amine solvent.[57] These conditions allow for fast reactions with good yields at room temperature or slightly elevated temperatures. The addition of copper does raise the reaction rate but allows for the Glaser-Hay homocoupling of terminal alkynes in the presence of oxygen.[58] To overcome this, Sonogashira coupling must be performed under an inert atmosphere to avoid by products. Recent advances in Sonogashira coupling focus mainly on 1.) the removal of copper catalyst, 2.) ligand structures, activity and 3.) use of Palladium nanoparticles.

Since the addition of copper by Sonogashira, there has been push to remove it from the reaction. Copper is known to facilitate side reactions in the presence of oxygen that can be avoided by just palladium catalyzed reactions. To get around this, protocols have been developed that increase the rate of homogenous palladium species. For instance, by replacing copper salts with $Pd(TPP)_3$ along with a stronger organic base (TBAB) inactivated iodoaryls are able to be coupled with phenylacetylenes.[34] As well, just increasing the loading of $Pd(TPP)_3$ to six mole percent over the normal two mole percent has been shown to afford conditions that will allow for good yields in relevant time scales.[35] By using encapsulated palladium complexes Handa et al. were able to use only water with triethylamine to drive couplings with both activated and inactivated substrates as well as bromides with good yields.[36] Also, Das et al. has shown that by adding highly substituted nitrogen-based ligands that copper can be removed with high yields for aryl iodide, bromide, and even chlorides under mild reaction conditions with long term air stability.[59] These cases are just a few to have successfully removed copper co catalyst but the removal limits the yield and rate in all cases over catalyzed systems.

In traditional cross coupling reactions such as Suzuki, Heck, Buchwald, and Sonogashira, the primarily catalyst is a homogenous ligated palladium catalyst. These ligands are designed to

afford reaction rate, stability, and selectivity. The major ligand class used in cross coupling reactions consist of phosphorous centers attached to aryl branches. These ligands are more commonly known as phosphine ligands. The main driver for phosphine ligands comes in two factors: steric size, and electron richness. For example, one of the most widely used ligands is triphenylphosphine.[60] This ligand is very large with three aryl groups directly attached to a central phosphorous molecule. The lone pair of phosphorous then interacts with palladium species donating into the complexes overall electron density. By increasing the density within the Pd center the oxidative addition of aryl halides can be greatly increased.[61] Of these two factors, bulk is the easiest by far to control. It has been shown that for phosphine ligands, the smaller the substrate to be coupled, the higher the reaction rate if a bulky ligand is used. The inverse is also true with reaction rates increasing as the bulkiness is reduced for substrates with higher steric hindrance.[62] The bulk of the phosphine ligands is captured in the cone angle or Tolman angle.[63] This angle is a measure of the angle from the Pd center to the edge of the ligand. Recent advancements have seen phosphine coupled with ionic ligands and formally charged anionic species.[64–66] This allows for ease of separation as traditional solvents can be used to easily separate the catalyst from the products through liquid-liquid extraction.

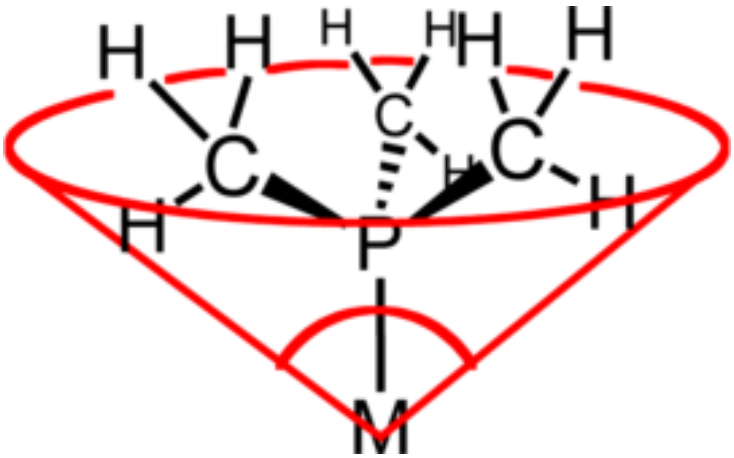

Figure 2.3.2 Triphenlyphosphine ligated to a metal center with the cone angle shown. From Tolman et al.[63]

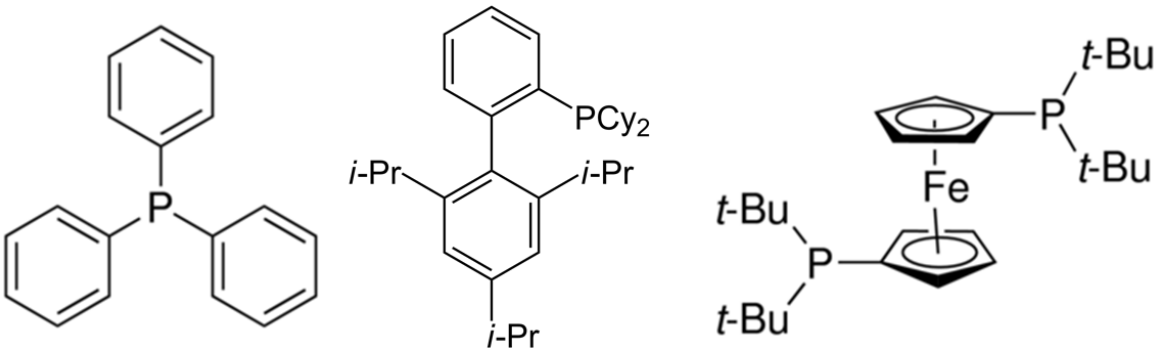

Figure 2.3.3 Common phosphine-based ligands. From left to right: triphenylphosphine (TPP), XPhos, 1,1'-Bis(di-tert-butylphosphino) ferrocene. Photos from Sigma Aldrich (prod num. 1.) T84409 2. 638064) 3.)701602)

Recently the advances in nanoparticle technology and use have moved into the space of cross coupling reactions. For homogenous catalysis, the reaction is finished when all reactants are converted in a given time period. After this process, the catalyst is either deactivated and removed or adsorbed onto charcoal and disposed of. This leads to high waste levels as well as high expenses for rare earth-based catalyst. Since homogenous palladium catalyst are environmentally unfriendly, toxic in final products, and expensive to use, palladium nanoparticles have risen to prominence as a way to reduce downstream processing and reduce overall cost by recycling the nanoparticles.[66] These particles though suffer from leaching of metallic species into solution under reaction conditions.[67] To trace this nanoparticle were filtered from solution and the supernatant was tested with ICP and AAS. There is one potential problem with this method though. It has been shown that leached atoms can reabsorb on the metal surface during the filtration giving the impression there is no leaching occurring.[68] One case of nanoparticle use is Pd-Fe core shell particles that were prepared and used for up to five cycles with no loss in activity. The particles are easily removed by magnetic fields applied to the reactor then resuspended.[69] These reactions can use copper as a co catalyst but again people have endeavored to make the system as simple as possible by removing copper salts. This limits the substrate scope as aryl bromides and chlorides have been shown to offer low to no yields even if activated.[70,71]

The reaction with more active iodoaryls has been shown to reduce as well with activated substrates demonstrating only moderate yields where with copper salts the yields were much higher.[72] While palladium nanoparticles look to be a premier replacement for homogenous catalysts, there is still much to be learned and understood about the mechanism of action under reaction conditions.

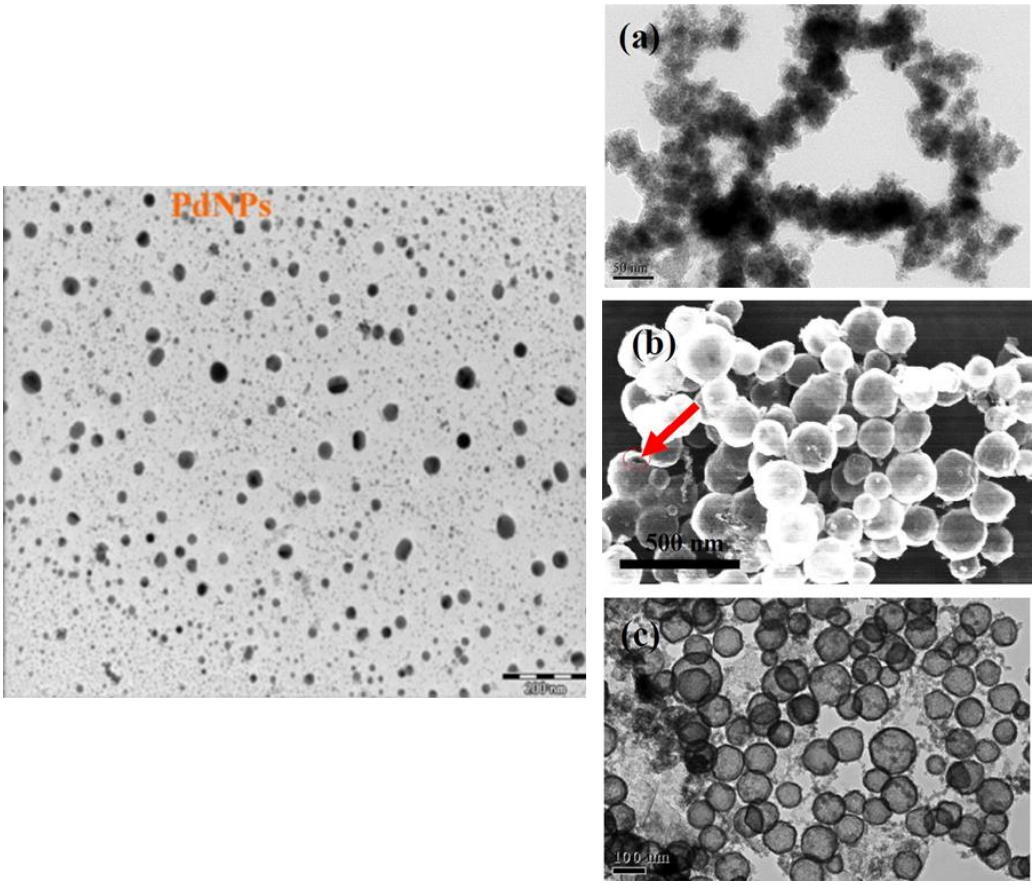

Figure 2.3.4 Representative images of palladium nanoparticles in TEM and SEM[72] 1.) Spherical Pd nanoparticles in TEM 2.) a.) TEM image of Pd-Fe nanoparticles b.)FESEM of Pd-Fe nanoparticles c.) TEM image of particle cross section showing hollow center. From Sawoo et al.[71]

Sonogashira coupling offers a convenient way of inserting a triple bond between two aryl groups without effecting other groups. The historic precedent has been focused on the development of copper free conditions as copper promotes Glaser Hay coupling. There has been

success in this path but the tradeoff has been found to be reaction rate. As well, phosphine ligand development has been a large focus due to the understanding of form and function. A profile of phosphine ligands has been developed to accommodate a variety of substrates from sterically hindered to electronically deactivated. Furthermore, palladium nanoparticles have seen a rise is popularity for ease of separation and lower cost of use. There is still large debate though over leaching and stability of these particles in reaction conditions.

CHAPTER III

Methodology

3.1 FDTD Simulations

Finite difference time domain (FDTD) simulations are a solving method to work out Maxwell's equations for electrical and magnetic fields on a nanoscale environment in the space and time domains.[73] Simulations were performed using the FDTD solutions software from Lumerical Inc. This software was used to estimate the optical response expected for a variety of shapes and sizes of plasmonic metal nanoparticles. The reported parameters from the software are extinction, absorption, and scattering coefficients across the visible and ultraviolet spectra of light. All optical properties used in the simulations were taken from an in-built database using data from Palik.[74] The boundary conditions used were periodic in the X and Y directions with perfectly matched layer (PML) used in the Z direction. The extinction cross sections were obtained by the use of a total field scatter field source (TFSF).[73] The light source wavelength depended on the simulations but all fall between 300-1000 nm. The background or index of simulations reported here are 1.333 or that for water, unless otherwise noted.

3.2 Copper Catalyst Preparation

Copper catalysts were prepared by using the microemulsion technique.[75] The technique uses n-heptane (99% Fisher Cat. No. AC447070025), polyethylene glycol-dodecyl ether (average Mn ~362, Sigma-Aldrich Cat. No. 235989), copper nitrate (99.999%, Sigma-Aldrich Cat. No. 229636), and hydrazine (98% Sigma-Aldrich Cat. No. 215155). Concisely, an aqueous solution

of copper nitrate (0.1 M) was added to a mixture of n-heptane and surfactant under stirring. The n-heptane/surfactant mixture was degassed with nitrogen prior to copper nitrate addition. After the addition of copper nitrate is allowed to settle, a 1M aqueous solution of hydrazine was dripped in drop by drop under stirring. The mixture is allowed to sit under an inert atmosphere at room temperature for the synthesis time. When finished a known amount of SiO_2 (Surface area ~80-100 m^2/g, Alfa Aesar, Product No. 42737) was added to mixture. The catalyst and silica were sonicated for twenty minutes to ensure good deposition on the surface. The solution was separated into centrifuge tubes where acetone was added to break the emulsion. The catalyst was washed twice then transferred to an oven to dry out at 70^{o}C overnight. Before use, the dry catalyst was calcined at 200^{o}C for 2 hours to ensure that any remaining surfactant was removed from the surface.

3.3 Analytical Measurements

3.3.a UV-Vis Measurements

All measurements taken are on an Agilent Cary 60. The dilution ratio varies depending on the sample of interest but in general the sample dilution for characterization of catalyst was 0.5 mL of catalyst preparation solution to 2.5 mL of absolute ethanol (200 proof). For reaction samples needing UV-Vis measurements a sample of 100 µL was taken from the reaction and diluted in 2 mL absolute ethanol. This sample was then diluted further by taking 0.5 mL into 2.5 mL of absolute alcohol (1:100). These dilutions ensure the response was well below the max absorbance of the instrument.

3.3.b GC-MS Measurements

The main method of quantification for this work is based on a Shimadzu QP2010SE GC-MS. This unit uses electron ionization (EI) to determine mass spectrums. Samples were prepared by taking 100µL of the reaction mixture and diluting into 10 mL of dichloromethane. The

samples were filtered through 0.22-micron filters before injection to ensure removal of any base or nanoparticles in the sample. Peak detection and integration were handled by the software provided by Shimadzu. Identification was verified using NIST spectral libraries with matching higher than 95%. No smoothing was used to process the samples to ensure accurate peak identification and quantification. Calibration curves were built independently using area vs concentration response from prepared reference samples.

3.3.c TEM Measurements

TEM was performed to help determine particle stability through average particle size. The samples were prepared by first selecting a carbon film copper grid that was unbent. The grid was supported using TEM tweezers. The sample was first sonicated for 1 min to break up any agglomeration of nanoparticles in solution. Then 10 µL was taken from the first UV-Vis sample and in one drop put onto the supported grid. The sample was allowed to dry in air for approximately 3 minutes. The excess solution was wiped away using stiff chem wipes. The measurements were performed on a JEOL-2100. The accelerating voltage was 200kV with a LaB_6 gun.

3.3.d High Resolution Electrospray Mass Spectroscopy

HR-ESI-MS was performed in order to characterize the homogenous compounds within the solution. The UV-Vis samples were used for this purpose. The samples were diluted in a ratio of 1:1 into a mixture of DCM (10mL), acetone (1 mL), and water (10 drops). This solution was used to ensure good spray characteristics. The samples were then injected into a LTQ Orbitrap XL mass spec. The spray conditions varied from each sample. The range of conditions though were 10-30 µl/min flow, 2-4 sheath gas, 0-3 aux gas, 3.0-5.0 kV spray voltage. The aux and sheath gas were both ultra-pure nitrogen at 100 psig. The machine was calibrated for negative mode prior to use each time.

3.4 Reaction procedure

Copper nanoparticles were synthesized by the microemulsion technique detailed above. They were suspended in DMF (15 mL) prior to starting the reaction (34.08 mg, 0.598 mmol). This mixture was added to a 25 mL round bottom with a condenser and thermocouple with a port closed by a glass stopper. Potassium carbonate was weighed out (207 mg, 1.64 mmol) and added while stirring the particles and DMF. Aryl halide (0.91 mmol) was added next while still stirring. The mixture was then heated for 15 min until it reached 110^{o}C. At this point phenylacetylene (0.91 mmol) was added and the reaction was started. The reaction was sampled as needed for GC analysis; therefore, the reaction time varied from 4 hrs to 24 hrs.

For hot centrifugation, Cu nanoparticles (34.08mg), DMF (15mL), potassium carbonate (207mg), iodobenzene (0.91 mmol), and phenylacetylene (0.91) were added using the procedure above. The mixture was allowed to react until 20% conversion of phenylacetylene was determined by GC-MS. The solution was then taken and centrifuged for 5 min at 3750 rpm and 40^{o}C to settle out all solids. The supernatant was then added to a fresh reactor and allowed to react at 110C until full conversion of phenylacetylene was determined.

CHAPTER IV

Findings

4.1 LSPR Spectroscopy as a Platform for Nanoparticle Stability by Utilizing FDTD Simulations[76]

In order to validate the use of LSPR spectroscopy for the purpose of catalyst stability I have chosen promising structures from literature; these structures include Pd cubes, Au spheres, Cu spheres, and Ag-Pd core shell spheres.[77–80] All of the listed nanostructures have been shown to be active for Suzuki, Heck, Sonogashira, as well as other coupling reactions. The use of FDTD simulations is employed to predict the extinction cross section of Pd cubes, Cu sphere, Au spheres, and Ag-Pd core shell spheres with varying levels of palladium thickness. Figure 4.1.1a-c shows the predicted extinction spectra for Pd cubes, Cu spheres, and Au spheres in water respectively. Pd cubes with an edge length of 15 nm were chosen in order to mimic proven catalytically active species found in coupling reactions.[77] For Au and Cu spheres 10 nm was chosen as the starting diameter since this size range has been shown to be catalytically active in cross coupling reactions. [78,79]The resonance peak seen at 300, 500, and 550 nm in Fig. 4.1.1a-c is the signature LSPR peak for Pd cubes, Cu, and Au spheres respectively. It is clear from Fig. 4.1.1d that the LSPR response is directly tied to the particle size. Through spectra analysis I was able to determine peak position, full width half maximum (FWHM), and extinction intensity change (See appendix for full analysis). For monometallic nanostructures, extinction intensity has been found to be a good descriptor for particle size. Figure 4.1.1d shows that for Au spheres in water as the particle size decreases the extinction intensity decreases as well. For instance, if an Au sphere loses just 0.5 nm from the surface, due to leaching, the LSPR intensity is predicted to decrease by 12%. In the case of most later transition metals with FCC structures, the loss of 0.5

nm can be equivalent to the loss of approximately a monolayer from the surface of the particles. For Cu spheres, and Pd cubes I observe similar trends of particle size to extinction intensity seen for Au spheres (full figures in appendix). Through analysis of these common proven active particles FDTD simulations have been shown to be able to determine catalyst stability (ie leaching). Furthermore, FDTD simulations show high sensitivity to surface changes and are able to quantify even the loss of a single monolayer from the surface.

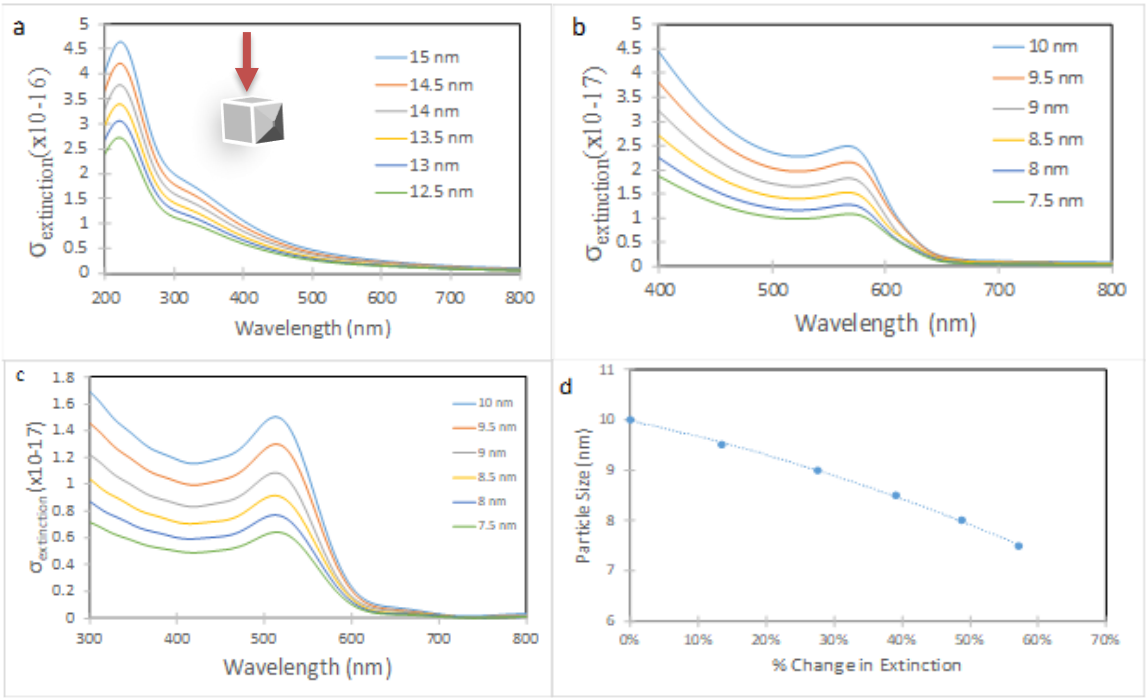

Figure 4.1.1 Simulated extinction spectra for a.) Pd nanocubes (light source is from top of the cube in the negative z direction) b.) Cu spheres c.) Au spheres all in water with periodic boundary conditions d.) Particle size versus percent change in extinction intensity for Au Spheres in water[81]

The extinction spectra of Ag-Pd core shell nanospheres simulated from 5 nm shell thickness to the Ag core are shown in Figure 4.1.2a. In order to show applicability of this method a 16 nm Ag core and a Pd shell of 5 nm was chosen to mirror a known active catalyst for C-C couplings.[80] For this core-shell arrangement I found that peak position and FWHM are good descriptors for determination of stability of the Pd shell. Figure 4.1.2c shows that as the Pd shell leaches into solution the peak will red shift to the Ag LSPR peak position. For the loss of 0.5 nm

of Pd from the surface, approximately 1 monolayer, the peak is predicted to shift 11 nm. This shift is well within the ability of modern UV-Vis spectrophotometers to determine. For FWHM the trend is similar. As the Pd shell is lost into solution the peak is predicted to sharpen until the Ag core is exposed. This shows that even for bimetallic structures LSPR spectroscopy tied with FDTD simulations can be used to predict stability.

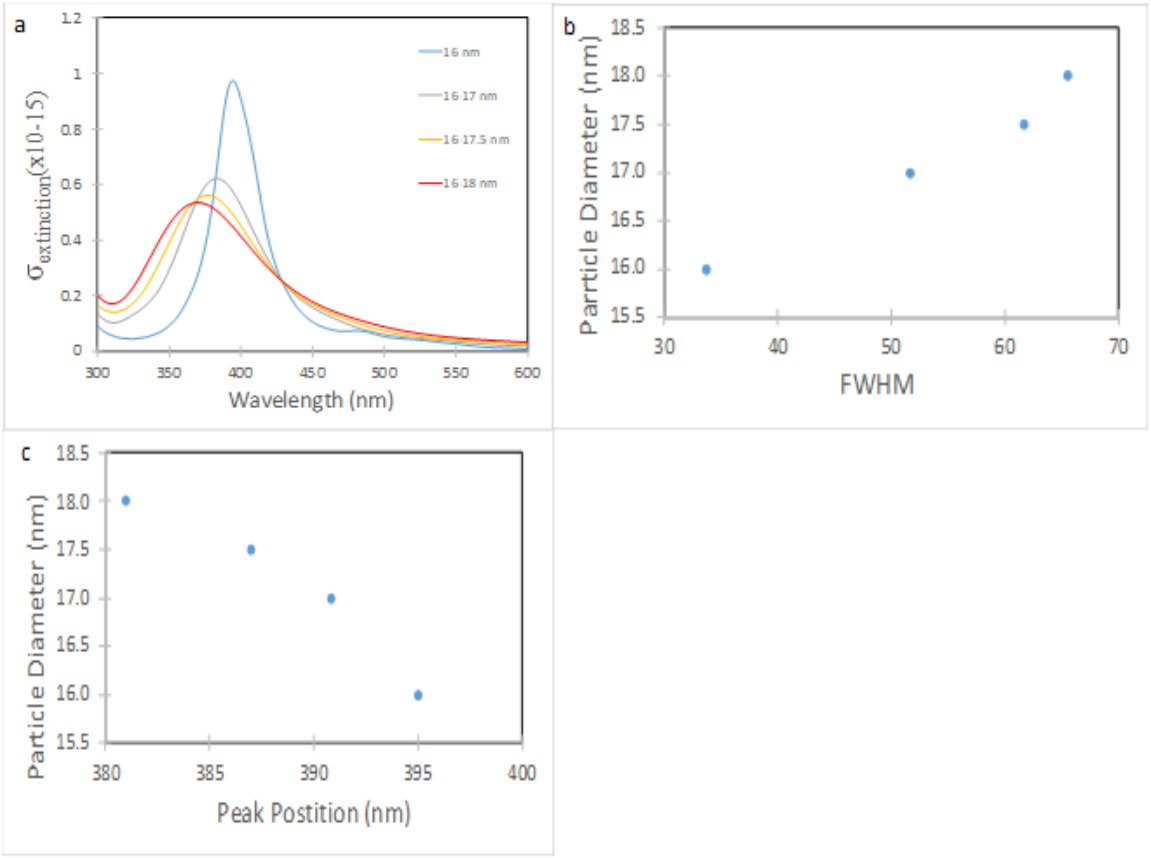

Figure 4.1.2 a.) Extinction spectra of Ag-Pd nanoparticles in water from 0-4.5 nm of palladium b.) FWHM for Ag-Pd particles versus monolayer thickness c.) peak position of the LSPR peak for Ag versus Pd shell thickness[81]

Using the FDTD simulations from Figures 4.1.1 and 4.1.2 show that if a nanostructure is stable under reaction conditions then UV-Vis spectra, i.e. extinction spectra, will show no major changes in the LSPR intensity for monometallic particles and peak shift/FWHM for bimetallic particles. The validate these simulated observations, we validated our results against the growth and leaching of gold spheres. The first was growth of gold particles under the seeded citrate

reduction method described in literature.[82] A full procedure may be found in the appendices. Briefly, in this approach seed particles are first prepared by reduction of Au precursor using sodium borohydride and ascorbic acid. The average size of the seed particles is 8.02 nm ± 0.59 nm determined by TEM. To follow the growth of gold particles a known amount of gold precursor was added to the seed solution while in operando UV-Vis spectra and TEM samples were taken. This allows for accurate comparison of LSPR response and particle size between simulations and experiments. Figure A4-7 show the results of this validation. For the growth of the Au particles, Figure A7 shows the fit between simulated and experimentally determined particle size versus the % change in the LSPR intensity. The fit is quite close indicating that the simulations predict the particle size determined by TEM without the need for costly analytical tools. The error bars shown represent the standard deviation of measure particle size. The standard deviation measured matches well against that shown for the synthesis method used.[82]

The second system used to validate the simulations is the leaching of Au into solution during oxidative homocoupling of phenylacetylene. To begin the reaction quasi-spherical particles with an average size of 12.32 ± 1.1 nm were added to a 83-17 vol/vol% mixture of water/DMF. Potassium carbonate was added followed by phenylacetylene. The solution was then heated at 85ºC under stirring to maintain particle suspension. Samples were taken from the reaction to determine LSPR intensity along with GC-MS yield of product, and TEM. Seen in Figure A8 the extinction spectra follow the expected trend from simulations for monometallic particles that are leaching into solution. It is seen that as the reaction proceeds that a second peak emerges at 480 nm. This appearance of a second peak demonstrates that phenylacetylene is adsorbing onto the surface and inducing leaching of Au atoms into solution forming homogenous metal species. To characterize this metal complex, ESI-MS was performed and found a potential match corresponding to $[Au(PA)_2]^-$ with a m/z of 399.2 amu. The spectrum obtained can be seen in Fig. 4.1.3. The peak seen at 480 nm is tentatively assigned to this species. The

presence of the soluble metal complex along with the formation of homocoupling product could indicate a homogenous reaction pathway. For determination of leaching, TEM samples were taken throughout the reaction. In order to determine the LSPR contribution in this case as opposed to growth the extinction spectra obtained was first deconvoluted to remove the complex addition. After deconvolution, the fit between simulated and experimental particle size versus % extinction change shown in Fig. A9 is quite close. As before, the error bars seen in the experimental samples represent the standard deviation of measured TEM samples. These standard deviations are expected from the synthesis method polydispersity. In order to quantify the closeness of the fit a parity plot was constructed for simulated versus experimental particle sizes. The slope of the best fit line was found to be 1.0067 with an R^2 value of 0.987. Since the slope and the R^2 are close to 1, the ability of FDTD simulations to predict particle size is confirmed allowing for a cost-effective way to determine catalyst stability without expensive analytical techniques.

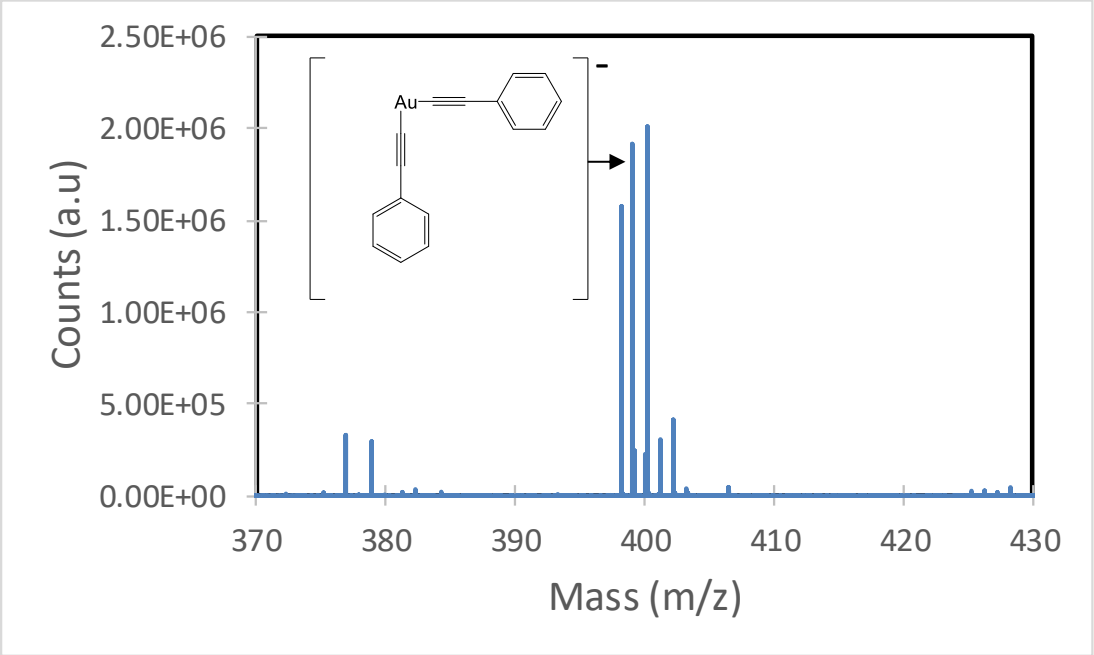

Figure 4.1.3 ESI-MS of oxidative homocoupling indicating a potential homogenous gold complex[81]

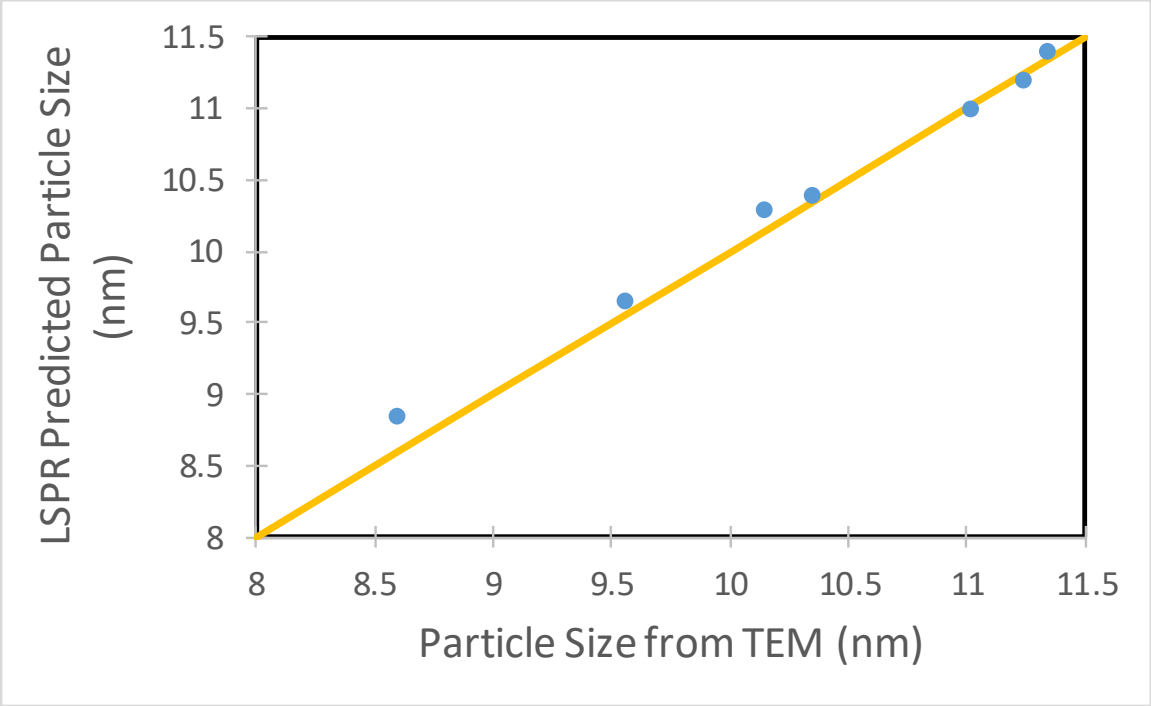

Figure 4.1.4 Parity Plot of simulated vs. experimentally determined particle sizes with a 1:1 line. R^2=0.986[81]

4.2 Determination of Energy Transfer Pathways in Cu_2O/Cu Nanostructures

Copper nanoparticles were synthesized via the microemulsion technique detailed above. Briefly, heptane and Brij-4 are mixed together under stirring. Then copper nitrate is added in a single volume. Hydrazine is then added drop wise while stirring. This ensures good reduction of particles and leads to a better dispersion. The mixture is allowed to stir for 18-24 hours while covered but under O_2 atmosphere. The presence of oxygen allows a shell of Cu_2O to form on the bulk Cu core. The typical particle size is 125-150 nm with a standard deviation of 12 nm. After synthesis, the particles are supported on fumed silica. The particles are washed with acetone to remove all of the Brij-4 which can decompose to carbon during processing. After washing, the particles are dried to yield a fine powder.

The particles have a thin layer of 3-4 nm of oxide with an approximate size of 125 nm measured by XRD and SEM respectively. To elucidate the energy transfer pathways via shell thickness control, the nanoparticles were placed in a tube furnace and packed with glass wool on either side. Hydrogen was then flowed at room temperature to purge out air for ten minutes. After this, the furnace was heated to 175°C in 2 minutes and held for 20 minutes. Subsequently, the furnace was cooled to room temperature with hydrogen flowing to help reduce the amount of oxygen contacting the nanoparticles at elevated temperatures. By following this procedure, the amount of oxide was able to be controlled. It was found that the oxide thickness was easier to control when reducing the shell off rather than adding shell with excess oxygen concentrations at higher temperature. The oxidation of Cu to Cu_2O or CuO even is a kinetically faster and thermodynamically favorable process so great control is needed to add only small layers without total oxidation. As well, I discovered at 175^oC the reduction can only reach a certain depth within the particle. This indicates a diffusion limited process associated with reduction of Cu_2O. After this depth is reached around 4 hours of hydrogen flow, the furnace is ramped to 200^oC to completely reduce the particles with confirmation by XRD.

To monitor the extinction spectra for the particles, diffuse reflectance measurements were taken using a Harrick scientific handheld DRA coupled with a Cary 60 UV-Vis spectrophotometer. During the partial reduction, I found that as the shell thickness decreased, the SPR peak for Cu emerges around 550 nm as expected. The peak intensity increases with each subsequent reduction of the oxide shell thickness. This peak is believed to be a higher order peak i.e. quadrupole. With progressive reduction though this peak remains relatively constant while the dipole peak increases from the baseline to a prominent peak.

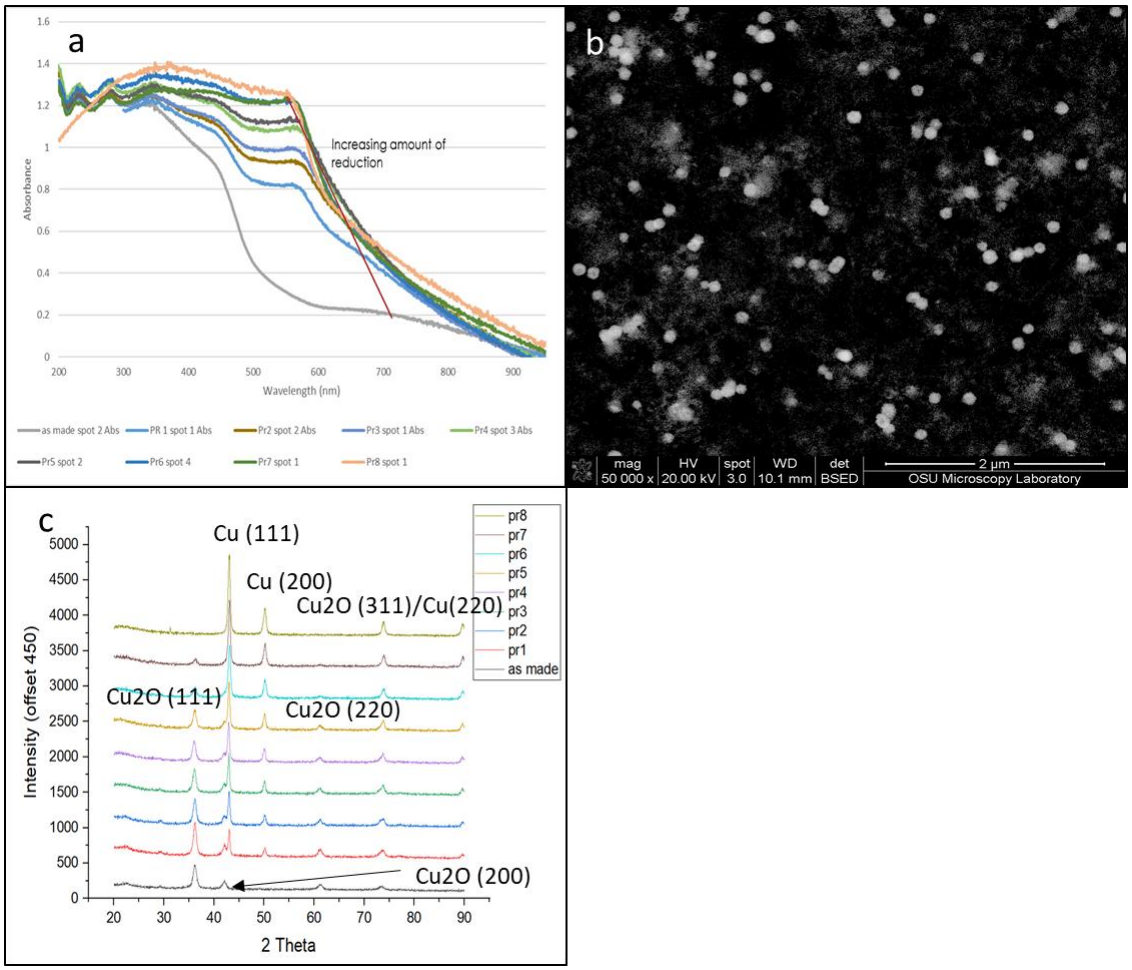

Figure 4.2.1 a.) DRA spectra of successively reduced copper nanoparticles on fumed silica b.) SEM backscatter image of Cu nanoparticles prepared on fumed silica support avg. particle size 110 nm c.) XRD spectra of Cu supported on fumed silica reduced at 175°C, with the final reduction at 200°C (Cu_2O peak from Kooti et al.[83] Cu peaks from Narushima et al.[84])

During the partial reductions, the copper spectra exhibited interesting features. The first of which is the appearance on a higher energy peak around 400 nm that is quite broad. This peak exhibits features dominated by the expected quadrupole of copper as well as the known interband transitions within copper states. These will be discussed in greater detail further on. The other feature that emerges is a small peak at a lower energy than the expected Cu core surface plasmon peak. By appearing below the surface plasmon for a spherical copper particle, this second peak indicates the presence of a thin shell of copper forming on the exterior of the particle as hydrogen reduction occurs. It has been shown for Au/SiO_2 as well as Ag/SiO_2 shell/core nanostructures that

as the shell thickness decreases the localized surface plasmon excitation is red shifted drastically.[85–87] The shell in this case is not very thin as the partial reduction is almost completed with only a very thin layer of Cu_2O left near the center of the particle. This is believed to lead to the appearance of a lower energy peak around 730 nm.

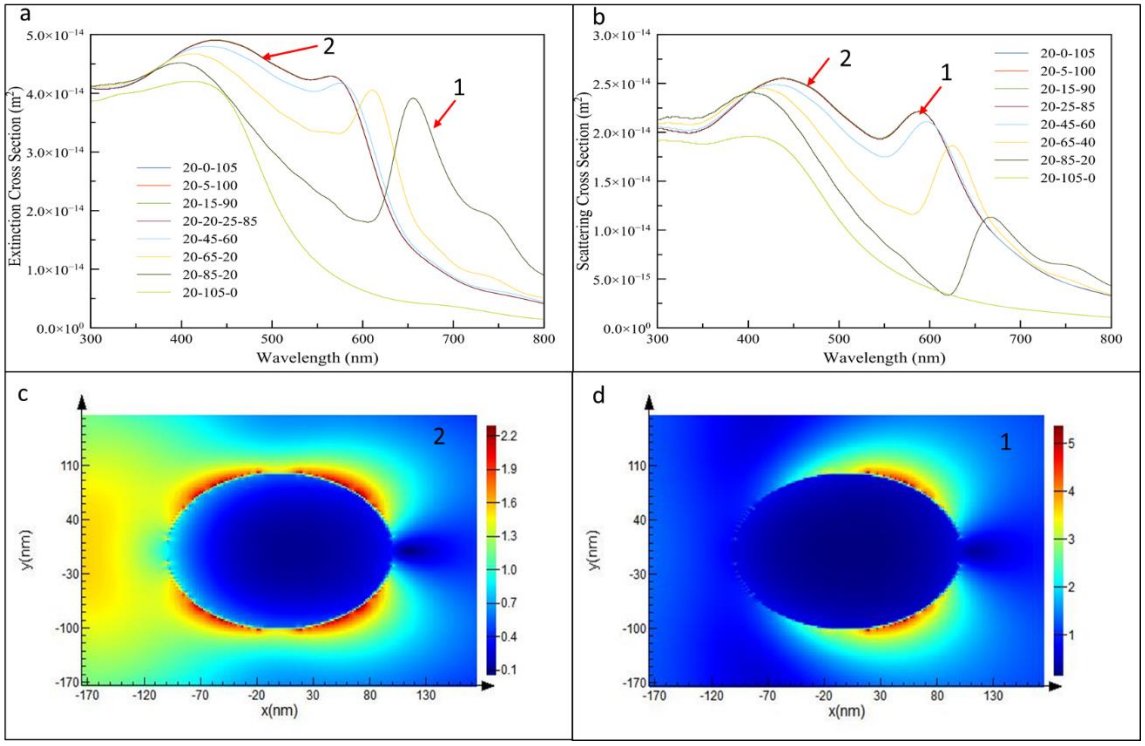

Figure 4.2.2 FDTD simulations of Cu/Cu2O/Cu particles with a 20 nm core in water with a Cu_2O shell and Cu outer shell. a.) Extinction cross section b.) Scattering cross section c.) electric field map for Cu particles excited at the quadrupole wavelength of 420 nm d.) electric field map for Cu particles excited at the dipole wavelength of 622 nm. Total field scatter field source was used to collect extinction and scattering spectral data. Plane wave source was used with PML boundary conditions to generate the electric field data[88].

To better understand reduction phenomena, FDTD simulations were used modeling the core as a static size with an increasing shell thickness and decreasing oxide layer thickness. Initially the particle starts as a 20 nm copper core with a shell of 125 nm Cu_2O, leading to an oxide layer thickness of 52.5 nm. This is set by using SEM imaging to get the total particle size. The core size was determined by fitting of experimental DRA to a range of simulated starting core sizes. This sweep yielded the representative core size of 20 nm in diameter. After setting the

starting size, increasing thickness of Cu shells was applied to simulate the partial reduction steps taken during this process. In doing so, we show that as the Cu_2O shell decreases i.e. the outer Cu film thickens, the surface plasmon peak blue shifts towards 570 nm which is the expected peak of Cu nanoparticles of 125 nm. As well, during experiments with decreasing amount of oxide the peak shape becomes sharper along with an increase in intensity. The intensity increase is expected as the amount of Cu present increases meaning a larger cross section for light interaction. The peak width or sharpening is believed to be due to the decrease in CID by the inner Cu_2O layer.

CID has long been understood to occur in LSPR as a mode of energy release to adsorbed molecules.[19,89] Briefly when this mode of energy transfer occurs the plasmon excitation energy matches that of the adsorbed species unoccupied energy levels. The energy is then able to transfer from the excited surface plasmon directly to the unpopulated states. After decaying into the vibrational modes of the adsorbate, the excited distribution falls back to the metal substrate (i.e. copper). This can happen for an adsorbed species with unpopulated electron states near the surface plasmon excitation energy, i.e. molecules, other metals, semiconductors. In Cu_2O/Cu core shell or Cu/Cu_2O/Cu shell/shell/core particles, this process is able to happen for both the inner core and the outer shell on the inner side. This is possible due to Cu_2O having close contact with the surface of the core and inner shell as well as the distance between the surface plasmon excitation energy and the conduction band of Cu_2O. Taking the known band gap for Cu_2O and the fermi level for Cu, the gap is found to be only 1.4 eV. This gap is easily surmounted by the LSPR of Cu which occurs at 1.9 eV above the Cu fermi level. In saying this, it is not without noting that DET is also possible to contribute to energy transfer as the band structure is quite close which allows for higher probability of transfer of sp electrons as well as d state electrons. If CID is playing a large role then as the samples reduce, i.e. less oxide to interface with, the peak for Cu is expected to sharpen (smaller FWHM), as well the peak position will blue shift towards the true

LSPR peak for Cu around 550 nm. Using Origin deconvolution software, I see this expected trend for the partial reductions of Cu_2O/Cu. The peak shift ranges from 743 nm to 547 nm. The FWHM is measured by fitting a Gaussian distribution to the peak since it is a population average known from SEM averages. The FWHM if found to range from 70 to 45. This indicates that as the sample becomes more reduced, that CID weakens between the Cu core Cu_2O shell and Cu outer shell. If DET were the dominate energy mechanism instead, the FWHM would be unaffected for DET while the LSPR peak would red shift. The combination of FWHM decrease and red shift makes CID unique to identify in the extinction or scattering spectra of LSPR materials. For RET to play a dominate role, the line shape is expected to decrease in intensity with no change in peak position. This is due to the surface plasmon oscillation causing the excitation of e/h pairs in the semiconductor valance band.[25]

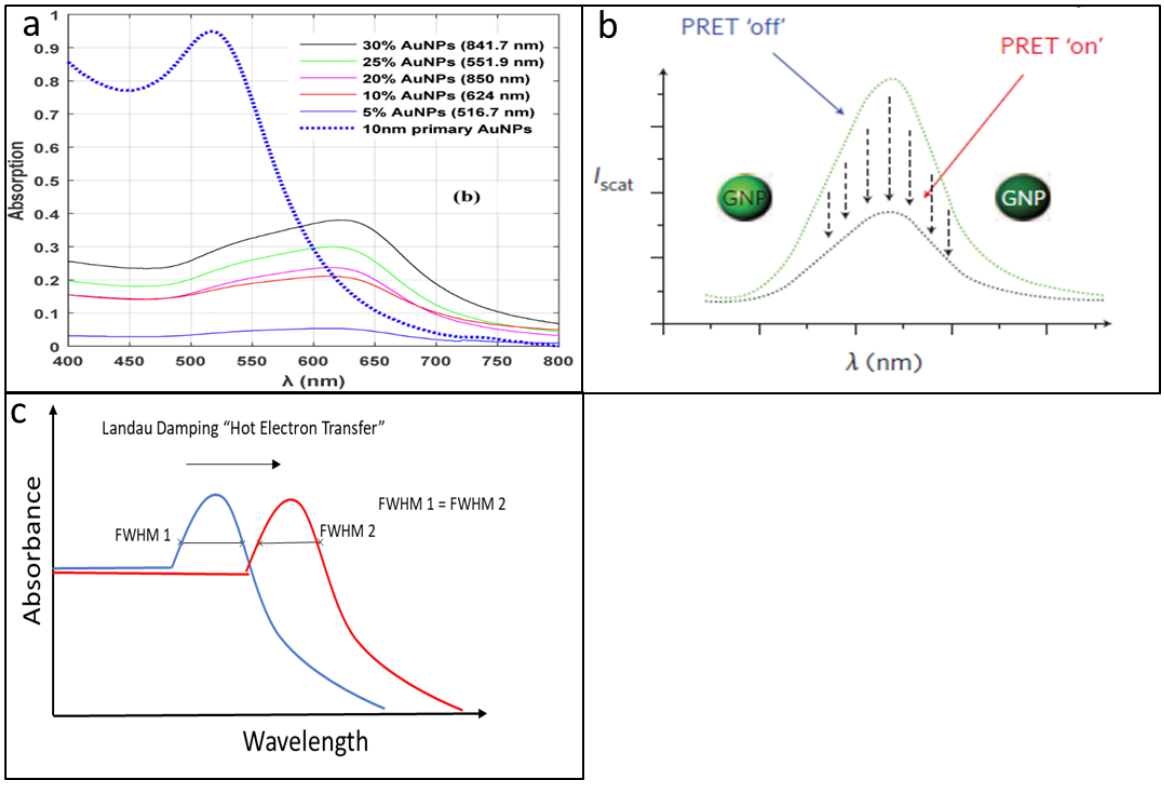

Figure 4.2.3 a.) CID response of Au nanoparticles in NaCl solution[90] b.) Resonant energy transfer line shape influence in gold nanoparticles[25] c.) DET line shape prediction[76]

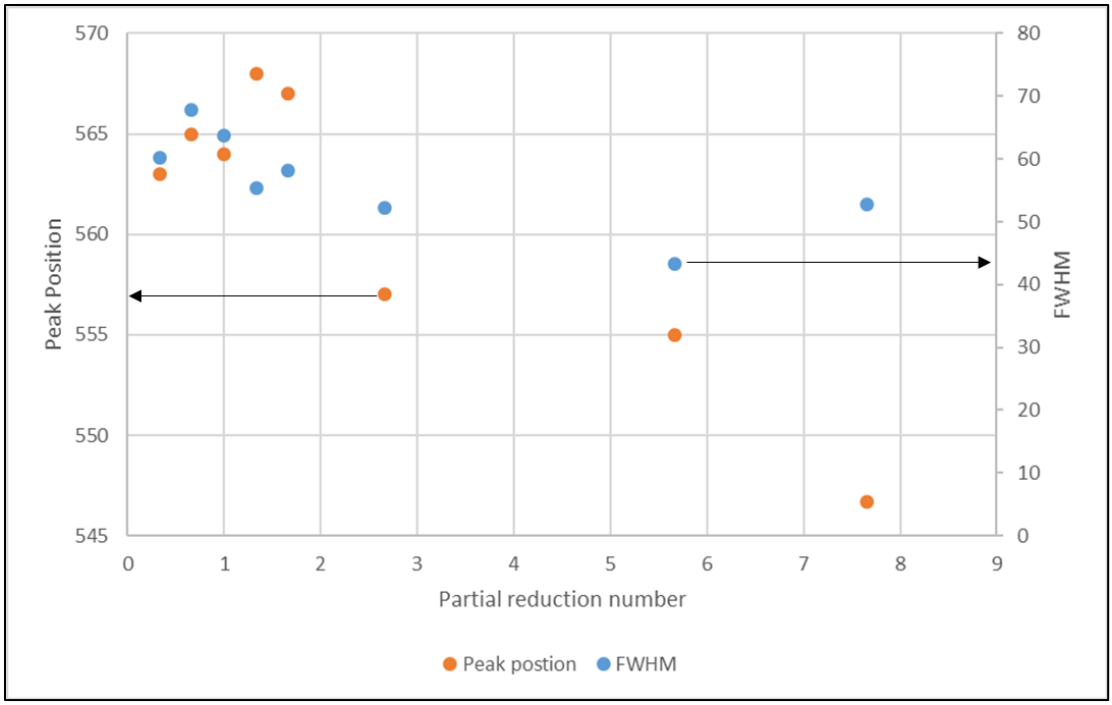

Figure 4.2.4 Deconvoluted peak position and FWHM determined by Gaussian fit curves. Notice both the peak and FWHM reduce with increasing amount of reduction time as expected of CID energy transfer.

One feature that is unexplained is a "cutoff" seen at 440-415 nm. This feature is only present in as made and samples known to contain large amounts of oxide. I propose potential the plasmonic nature of large Cu_2O nanoparticles. Surface plasmon resonance is not a select phenomenon that happens only to metals. It happens that Cu, Ag, Au have conditions favorable to show resonance in the UV-Vis region of light. For surface plasmon resonance to occur, the collective electron distribution must oscillate in the incident electric field. This oscillation is dependent on material properties, surrounding medium, as well as size of the particles. Using FDTD simulations with experimentally gathered n,k data[91], I have shown that for larger Cu_2O particles a peak appears with a sharp cutoff around 440 nm. The peak only appears in larger samples of Cu_2O consistent with what is seen from experimentally determined particle sizes of around 125-150 nm. To confirm the simulated results several steps are taken. First, the material data fit was checked within the software. The program uses a fitting algorithm to convert discrete experimental data into a continuous equation used for calculations. If this fit is not good, the

algorithm can throw artificial peaks causing a false positive. I analyzed the fit done by the algorithm and found it to be adequate with no large deviations that could cause the peaks to appear. The next step in confirming the simulation fit is to use field monitors to analyze the peak scattering pattern. For surface plasmon resonance since the cloud is oscillating the scattering of the particles will be displaced or separated across planes. This leads to dipole and higher order separation patterns in the electric field seen around the particles. Using monitors within FDTD simulations, I have shown that Cu_2O does in fact have both dipolar and quadrupolar modes. This helps to confirm that the "cutoff" is potentially the LSPR of Cu_2O. To truly determine this, experiments analyzing lifetime of the event as well as electron distribution are needed. Overall, the "cutoff" feature seen in the scattering measurements has two possible explanations with both leading to plausible outcomes. This feature calls for future work to be pursued in this direction.

4.3 Copper based Ligand and Palladium Free Sonogashira Coupling[92]

In order to study copper nanoparticles in Sonogashira coupling, iodobenzene with phenylacetylene was chosen as a model coupling system. These coupling partners were used with DMF as the solvent and potassium carbonate as the base. Potassium carbonate was chosen due to good solubility in DMF compared to other inorganic bases as well as availability versus cesium carbonate. The nanoparticles were prepared separately using a microemulsion technique detailed above (3.1) and added with the solvent. The reaction was carried out at 110°C under air.

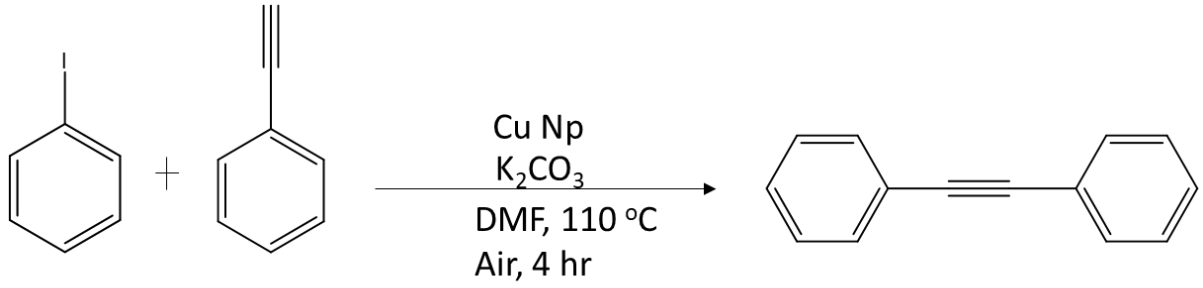

Figure 4.3.1 Scheme 2 Sonogashira coupling between iodobenzene and phenylacetylene

The reaction was sampled regularly for TEM, UV-Vis, and GC-MS analysis. The reaction was completed in four hours with the primary product homocoupling of phenylacetylene to diphenyldiacetylene. The final selectivity of hetero coupling product was 40%. This is believed to be due to Glaser-Hay coupling in the presence of oxygen. By running in a nitrogen blanketed environment this pathway can be avoided. When the reaction was run under reflux conditions(~147ºC) and the selectivity was increased to 90% with respect to the hetero coupling product.

During the reaction, a complex appeared in the UV-Vis spectrum centered at 450 nm. Organometallic complexes of copper are common in this region; mainly complexes of Cu^{2+}. This points to a homogenous mechanism for the reaction pathway. While homogenous mechanisms are well understood, leaching of metal oxides to form these complexes is less so. Panova et al. recently proved that in sulfur based cross couplings Cu_2O particles leach into solution and react via a homogenous pathway.[93] It was found during this study that the leached particles ligate with the thiol reagents regardless of the size, shape, surface facets of the nanoparticles. Indicating that the leaching is not facet selective but acts indiscriminately over the exposed oxide surface.

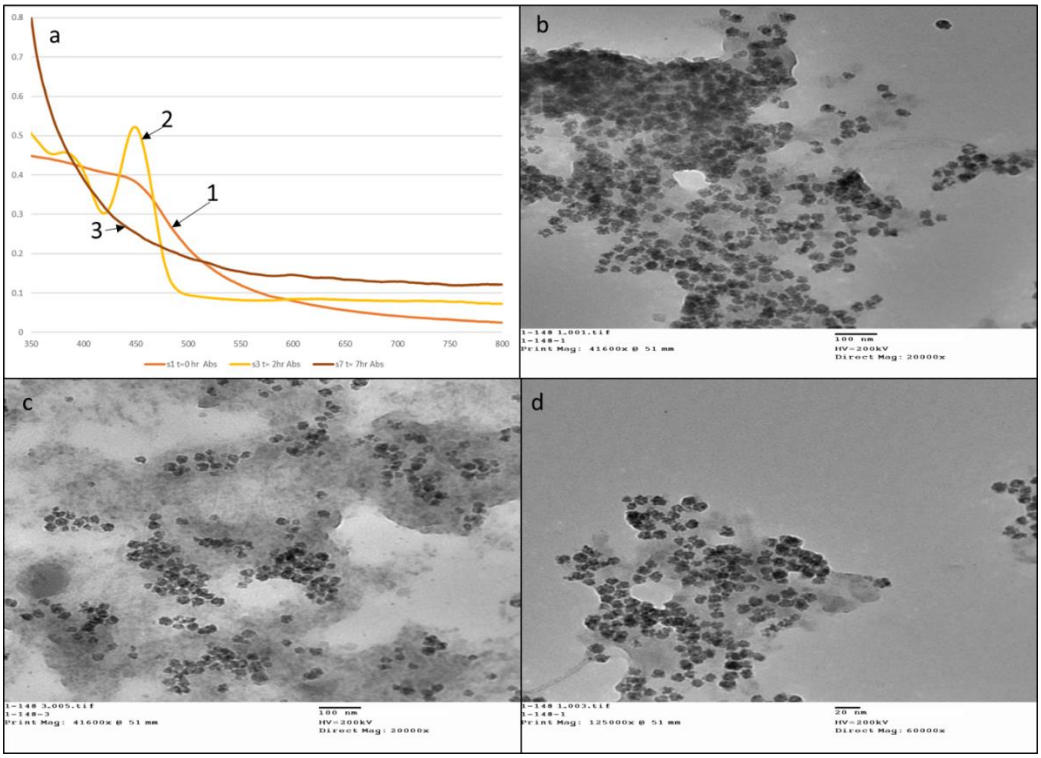

Figure 4.3.2 a.) Representative UV-Vis spectra of 1.) start of the reaction 2.) highest complex peak 3.) end of reaction b.) TEM image of Cu particles at the beginning of the reaction average particle size 26 nm c.) TEM of image Cu particles taken at point 2.) average particle size 22 nm d.) TEM image of Cu particles at the end of the reaction point 3.) average particle size 19 nm.

Using TEM to confirm that the particles do in fact leach into solution, nanoparticle sizes were sampled throughout the reaction. It was seen that the particles on average start around 130 nm in size. As the reaction proceeded, the particle size continued to decrease to an average of 5-10 nm. To confirm why this happens, experiments were performed without each reactant (phenylacetylene, iodobenzene). For reactions containing no phenylacetylene, it was found that the particle size was maintained around 130 nm throughout the reaction. When phenylacetylene was added, the particle size decreases similarly to model reaction conditions. This indicates that the terminal triple bond is responsible for the leaching of the metal atoms from the surface of the particles. It is worth noting that no homocoupling of iodobenzene was observed during this reaction.

Since leaching was confirmed by both TEM and UV-Vis results, hot centrifugation was used to determine if in fact there was homogenous species present that could carry out the reaction. The reaction was charged with nanoparticles and allowed to react till 15-20% conversion then centrifuged at 40°C to preserve solubilities. The supernatant was transferred back and allowed to continue the reaction. The reaction proceeded to complete conversion of phenylacetylene in four hours as before. After this first cycle was completed, base and reactants was added to see if the homogenous catalyst could cycle. The second cycle proceed to full conversion of phenylacetylene within 4 hours as in the first cycle; demonstrating the homogenous species does in fact cycle and is reusable. This indicates that there is in fact a homogeneous copper complex performing the reaction. Furthermore, the ability to run both hetero and Glaser-Hay coupling reactions indicates that the complex is able to catalyze both reactions.

To determine the structure of the homogenous complex, high resolution electrospray mass spectroscopy was used. ESI-MS in negative spray mode identified a complex with isotopic ratio of copper at m/z=281.24. The mass is found to add up to $[CuO(PA)_2]^-$. This complex at 281 indicates that a phenylacetylene binds to the surface of Cu_2O then the second equivalent comes in and removes a [CuO] unit into solution. The limitation of this method is that neutral species or species that cannot carry a formal negative charge are unable to be seen by the detector. As well, reactions were performed in absence of base and iodobenzene. In the reactions performed with no iodobenzene, the only product detected was diphenyldiacetylene (DPDA) formed through Glaser-Hay coupling. The complex at 281 was also present, indicating that the base is needed to cause the leaching into solution by removing the hydrogen from the surface. Bubbles are also visible in a knockout vessel, indicating the degradation of carbonates into carbon dioxide and water. Thereby indicating the uptake of terminal alkyne hydrogens.

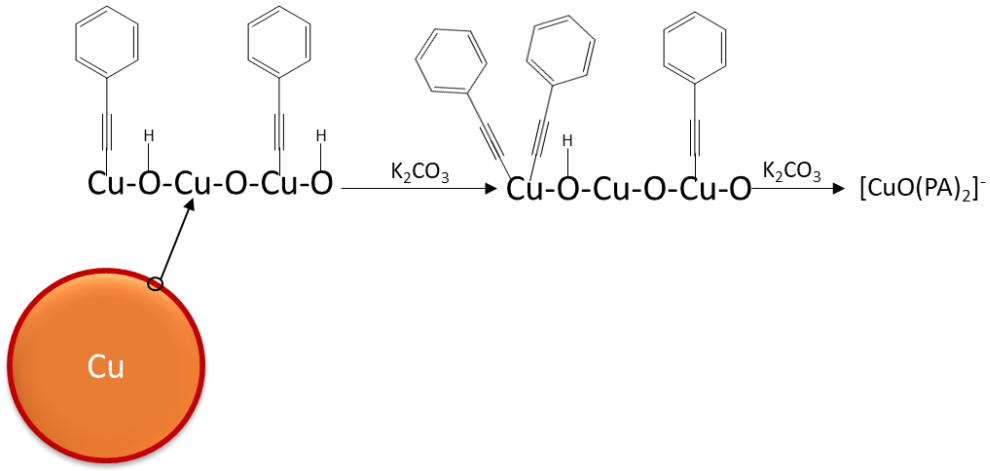

Figure 4.3.3 Schematic of leaching of Cu_2O from the nanoparticle surface and subsequent formation of the homogenous complex by phenylacetylene and base

To determine the applicability of this system, different substituted aryl halides were tested. The addition of electron withdrawing groups (EWG) sped the reaction up as well as increased selectivity towards hetero coupling. The addition of electron donating groups (EDG) has long been used with traditional palladium catalyst as a way to speed up the cross coupling. In this case, the reaction rate slowed when compared to no substitution; as well, the selectivity towards hetero coupled product fell. No aryl halide homo coupling was detected by GC-MS analysis for either group. It is worth noting only phenylacetylene was tested for terminal alkynes in this study due to the large demand for aryl substitutions over chains or simpler ring structures.

Entry	Aryl Halide	Terminal Alkyne	Product (Yield)
1	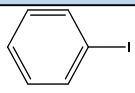 (1a)	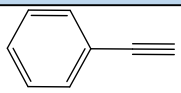 (1b)	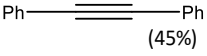 (45%)
2	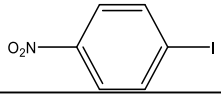	1b	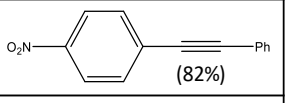 (82%)
3	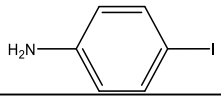	1b	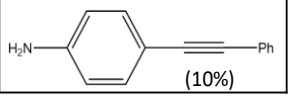 (10%)

Table 1 Summary of cross coupling reactions performed with various alkyne and aryl halides. Reaction conditions for all are 0.91 mmol of aryl halide and alkyne, 1.64 eq. base, 110°C, 15 mL DMF as solvent under air

Taking the information gathered from this model reaction and substituent studies, I propose the mechanism for this reaction starts with the nanoparticles giving up the oxide surface in the presence base to $[CuO(PA)_2]^-$. This is the starting form of the catalyst. The next step involves single electron transfer (SET) from the Cu^{1+} to the aryl halide to give Cu^{2+} and an unstable aryl ring. The iodine then leaves with the transferred electron giving an iodine ion and the aryl inserts to form $[CuO(PA)_2Ar]$. This complex undergoes reductive elimination to produce the cross coupled product and [CuO(PA)]. The Cu can then oxidize with base and phenylacetylene to return to $[CuO(PA)_2]^-$. The single electron transfer mechanism is proposed over radical propagation and oxidative addition/ reductive elimination, due to the large shift in peak position for this system in UV-Vis spectroscopy during the reaction. When the aryl halide is absent from the reaction there is no peak shift seen in UV-Vis. This peak always red shifts during the course of the reaction with aryl halide present. It is well known that as a compound extends conjugation, the peak red shifts due to the lowering of the pi to pi* and n to pi* transitions.[94–96] This indicates the formation of complex 3 in the schematic below. Complex 2 is then responsible for the primary peak seen during the reaction as the leaching and electron transfer is quick compared to the addition of the aryl halide. For aryl halides with EWG, the peak shift is much greater as more electrons can be transferred with far greater stability into the benzene ring. For

EDG then, the peak shift is minimal as in the case with no aryl halide. These observations lead me to conclude a SET pathway in the homogenous cycle.

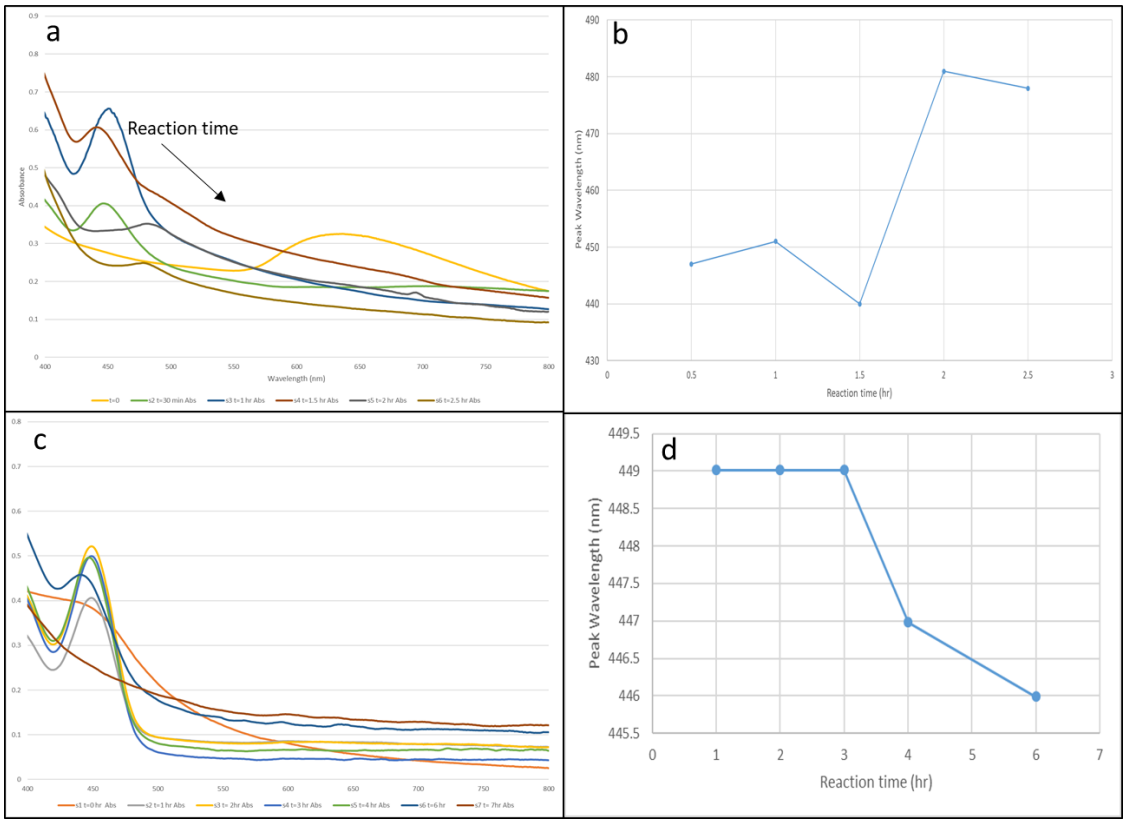

Figure 4.3.4 a.) UV-Vis spectrum of Sonogashira coupling between phenylacetylene and para-nitroiodobenzene (1eq) at 110C. b.) peak position of homogenous complex over the course of the reaction the large red shift c.) UV-Vis spectrum of Sonogashira coupling between phenylacetylene and iodoaniline (1 eq) d.) Peak position over the reaction time showing little red shift indicating a low formation of complex 3.

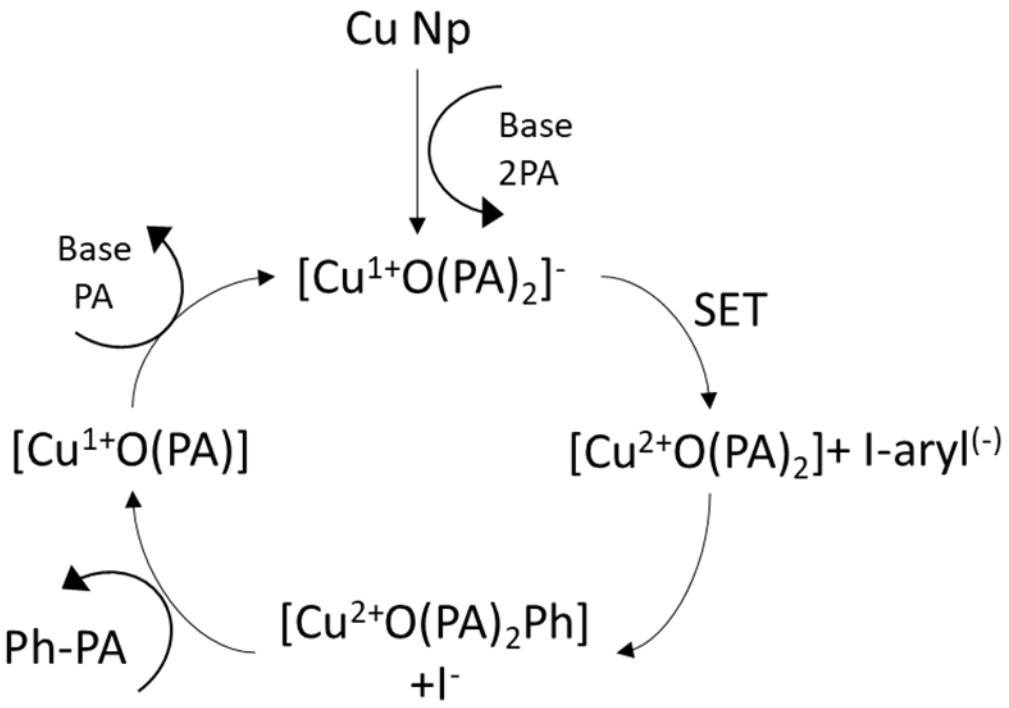

Figure 4.3.5 Proposed Mechanism of Cu NP catalyzed Sonogashria coupling with homogenous complexation and single electron transfer as the primary catalytic pathway

Since base lead to the leaching of the particles into solution I wanted to test the performance of the reaction without base. Two reactions were considered; first is the cross coupling with iodobenzene under nitrogen. Second is the homocoupling of phenylacetylene. These two represent model cases that can be expanded on later. In the first reaction all of the reagents were added as before with the exception of base. The reaction was run to completion over 24 hours. The selectivity towards DPA was measured to be >95%. The ability of this reaction to complete indicates that in the absence of base the reaction might proceed heterogeneously. Figure 4.3.6 shows that in UV-Vis spectra no complex is seen yet the reaction is able to proceed. To confirm these results, Glaser-Hay coupling of phenylacetylene was performed under aerobic conditions. The reaction was able to complete in 4 hours similar to the homogenous case. Similar to heterocoupling, there was no formation of a homogenous complex detected. This indicates that phenylacetylene is able to bind to the surface and react to form

DPDA. Taking both of these reactions together, this would indicate that in the absence of base copper nanoparticles are able to catalyze both Sonogashria coupling and Glaser-Hay coupling.

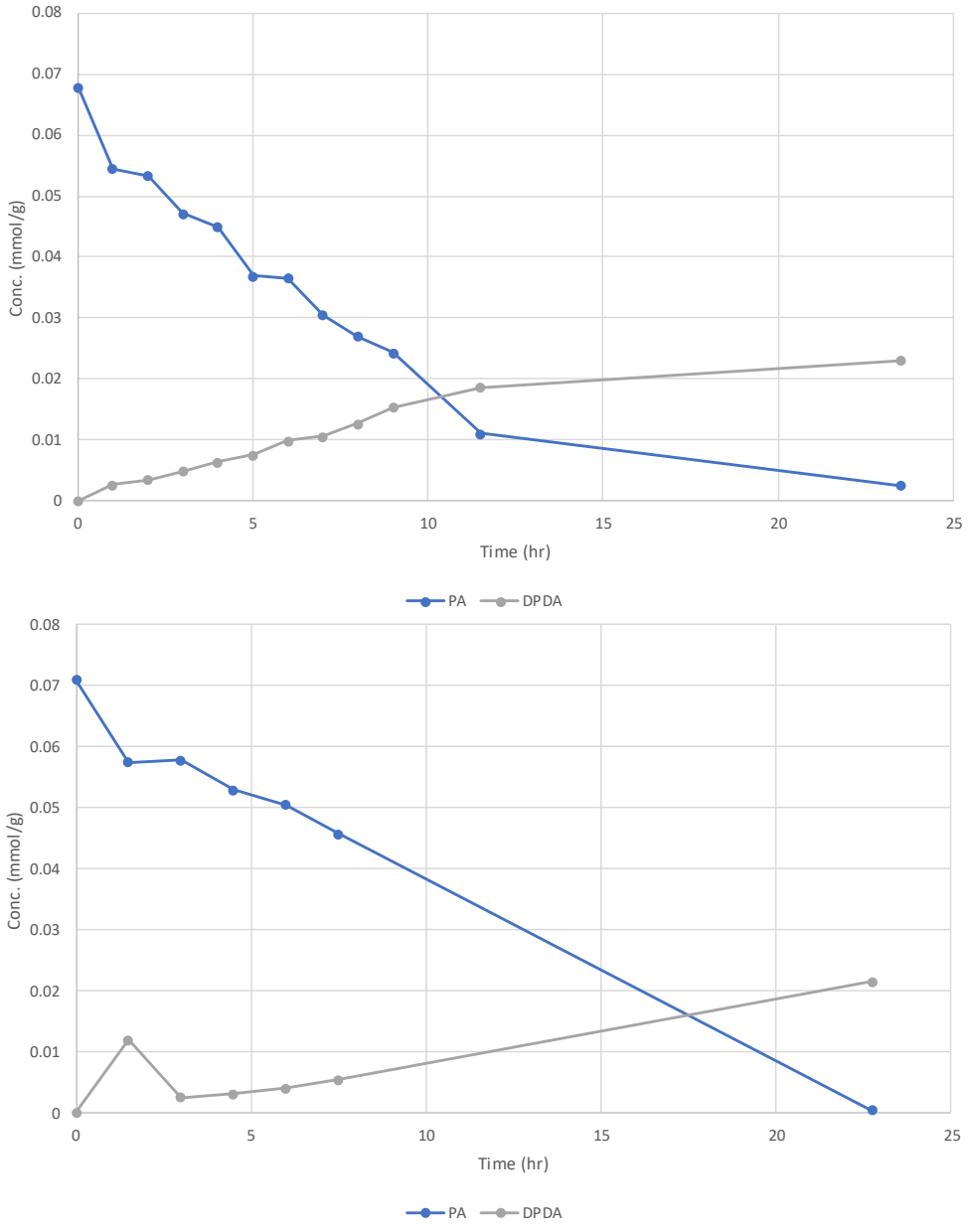

Figure 4.3.6 a.) (top) Homocoupling with phenylacetylene, base, and catalyst at 110°C under air. (bottom) Homocoupling without base only phenylacetylene and catalyst at 110°C under air.

CHAPTER V

Conclusions

5.1 Modeling of Nanoparticles and Nanoalloys

I have shown that by using FDTD simulations with LSPR spectroscopy, predictions of particle size and shape may be made with high accuracy. I have demonstrated for gold growth and under relevant reaction conditions that FDTD simulations correlate closely to experimentally determined particle size as well as LSPR response. I predict that for other particles such as Ag, Cu, and Pd-Ag structures this correlation will continue. By combining FDTD simulations and LSPR spectroscopy we have demonstrated a new method to track stability and understand homogenous versus heterogenous pathways in plasmonic metal nanocatalyst for relevant cross coupling reactions.

5.2 Control of Oxide Thickness on Cu_2O/Cu via Partial Reduction

I have shown by using a simple system of Cu_2O/Cu nanoparticles the energy transfer mechanisms between plasmonic metals and semiconductors can be better understood. Due to the overlap between the surface plasmon excitation and unfilled conduction band states of Cu_2O, chemical interface damping (CID) is shown to dominate over DET and RET. By measuring the extinction and scattering response of bulk supported particles it was shown that selective interactions occur at wavelengths where energy resonance is predicted between SPR and conduction band energy for Cu_2O. The presence of red shifting along with peak broadening as opposed to just red shifting for DET, and peak height decrease for RET, indicates that CID plays

the dominate role in the energy transfer process between Cu_2O/Cu structures. This is the first time this level of understanding can be gleaned from both experimental and computational work.

By understanding the fundamental energy transfer pathways in these systems, rational design of future light harvesting and photocatalyst bimetallic structures becomes much easier. Using the insights gained from this work, determination of viable systems as well as energy transfer potentials in these systems. Overall, while DET and RET are still a possibility in these bimetallic systems, chemical interface damping is shown to be the dominate effect when overlap between the surface plasmon and the conduction band occurs for a given semiconductor. This means that surface plasmon energy can be transferred directly yielding better efficiencies and higher levels of energy than Landau damping or RET. As well, I have shown that the reduction of Cu_2O occurs from the outside of the particle allowing for future work focusing on tunable shells by reduction methods.

5.3 Copper based Ligand and Palladium Free Sonogashira Coupling

We have demonstrated a palladium free, ligand free Sonogashira coupling protocol utilizing copper nanoparticles as a precursor. In this work we synthesized and characterized Cu nanoparticles as a potential catalyst for C-C bond forming reactions. It was found that in fact the nanoparticles under reaction conditions serve only as a sink for homogenous copper organometallic catalyst that perform the reaction. This is evidenced by TEM, UV-Vis, and ESI-MS results. In TEM particle size was seen to decrease with the addition of phenylacetylene indicating the terminal alkyne is responsible for leaching from the particles. UV-Vis confirms this by showing a large absorbance peak in the region of 450 nm. In ESI-MS the mass of the complex was determined to be 281.24 amu. This mass indicates $[CuO(PA)_2]^-$ as the initial state of the homogenous catalyst. This structure indicates that the phenylacetylene binds to the surface of the particles and by hydrogen extraction and the addition of a second alkyne group a CuO unit is removed into solution. The mechanism is shown to follow single electron transfer to aryl halides that then couple with the complex before being eliminated as cross coupled product. Furthermore,

without the addition of base the reaction is shown to proceed heterogeneously on the Cu2O surface. This is the first case of a nonpalladium, base free, heterogeneously catalyzed cross coupling reaction.

This system shows great potential for reduction of waste footprints in industrial applications. As well the functional group tolerance is understood then as EWG promote the SET donation much more strongly than EDG do. By understanding the mechanism and implications there-of, other reactions may be explored in the future to expand the use of cheaper more available catalyst in the field of cross couplings.

REFERENCES

(1) Challener, C. A. New Horizons for Cross-Coupling Reactions http://www.pharmtech.com/new-horizons-cross-coupling-reactions (accessed May 29, 2018).

(2) SG8 9AZ. (01763) 222 333, B. P. L., The Sty, 47 Upper King Street, Royston, Hertfordshire. Palladium Impurity Removal from API Process | Scale-up https://www.technology.matthey.com/article/60/4/277-286/ (accessed May 29, 2018).

(3) Flahive, E. J.; Ewanicki, B. L.; Sach, N. W.; O'Neill-Slawecki, S. A.; Stankovic, N. S.; Yu, S.; Guinness, S. M.; Dunn, J. Development of an Effective Palladium Removal Process for VEGF Oncology Candidate AG13736 and a Simple, Efficient Screening Technique for Scavenger Reagent Identification. *Org. Process Res. Dev.* **2008**, *12* (4), 637–645.

(4) Removal of Palladium from Organic Reaction Mixtures by Trimercaptotriazine - Organic Process Research & Development (ACS Publications) https://pubs.acs.org/doi/10.1021/op970107f (accessed May 29, 2018).

(5) Kidwai, M.; Bansal, V.; Kumar, A.; Mozumdar, S. The First Au-Nanoparticles Catalyzed Green Synthesis of Propargylamines via a Three-Component Coupling Reaction of Aldehyde , Alkyne and Amine. *Green Chem.* **2007**, *9* (7), 742–745.

(6) Wei, C.; Li, Z.; Li, C.-J. The First Silver-Catalyzed Three-Component Coupling of Aldehyde, Alkyne, and Amine. *Org. Lett.* **2003**, *5* (23), 4473–4475.

(7) Ma, D.; Zhang, Y.; Yao, J.; Wu, S.; Tao, F. Accelerating Effect Induced by the Structure of α-Amino Acid in the Copper-Catalyzed Coupling Reaction of Aryl Halides with α-Amino Acids. Synthesis of Benzolactam-V8. *J. Am. Chem. Soc.* **1998**, *120* (48), 12459–12467.

(8) Beaumont, S. K. Heterogeneously Catalyzing C–C Coupling Reactions with Precious Metal Nanoparticles. *J. Chem. Technol. Biotechnol.* **2018**, *87* (5), 595–600.

(9) Evidence for the Surface-Catalyzed Suzuki–Miyaura Reaction over Palladium Nanoparticles: An Operando XAS Study - Ellis - 2010 - Angewandte Chemie International Edition - Wiley Online Library https://onlinelibrary.wiley.com/doi/abs/10.1002/anie.200906675 (accessed May 29, 2018).

(10) Ji, Y.; Jain, S.; Davis, R. J. Investigation of Pd Leaching from Supported Pd Catalysts during the Heck Reaction. *J. Phys. Chem. B* **2005**, *109* (36), 17232–17238.

(11) Zhao, F.; Bhanage, B. M.; Shirai, M.; Arai, M. Heck Reactions of Iodobenzene and Methyl Acrylate with Conventional Supported Palladium Catalysts in the Presence of Organic and/and Inorganic Bases without Ligands. *Chem. – Eur. J.* **2018**, *6* (5), 843–848.

(12) Chinchilla, R.; Nájera, C. The Sonogashira Reaction: A Booming Methodology in Synthetic Organic Chemistry. *Chem. Rev.* **2007**, *107* (3), 874–922.

(13) A review of the problem of distinguishing true homogeneous catalysis from soluble or other metal-particle heterogeneous catalysis under reducing conditions - ScienceDirect https://www.sciencedirect.com/science/article/pii/S1381116902007288 (accessed May 29, 2018).

(14) Chaudhari, R. V.; Jaganathan, R.; Kolhe, D. S.; Emig, G.; Hofmann, H. Effect of Catalyst Pretreatment on Activity and Selectivity of Hydrogenation of Phenylacetylene over Palladium/Carbon Catalyst. *Ind. Eng. Chem. Prod. Res. Dev.* **1986**, *25* (2), 375–379.

(15) Lee, S.-K.; Hsu, H.-C.; Tuan, W.-H. Oxidation Behavior of Copper at a Temperature below 300 °C and the Methodology for Passivation. *Mater. Res.* **2016**, *19* (1), 51–56.

(16) Liu, G. L.; Long, Y.-T.; Choi, Y.; Kang, T.; Lee, L. P. Quantized Plasmon Quenching Dips Nanospectroscopy via Plasmon Resonance Energy Transfer. *Nat. Methods* **2007**, *4* (12), 1015–1017.

(17) Lakowicz, J. R.; Shen, Y.; D'Auria, S.; Malicka, J.; Fang, J.; Gryczynski, Z.; Gryczynski, I. Radiative Decay Engineering: 2. Effects of Silver Island Films on Fluorescence Intensity, Lifetimes, and Resonance Energy Transfer. *Anal. Biochem.* **2002**, *301* (2), 261–277.

(18) Li, J.; Cushing, S. K.; Meng, F.; Senty, T. R.; Bristow, A. D.; Wu, N. Plasmon-Induced Resonance Energy Transfer for Solar Energy Conversion. *Nat. Photonics* **2015**, *9* (9), 601–607.

(19) Hendrich, C.; Bosbach, J.; Stietz, F.; Hubenthal, F.; Vartanyan, T.; Träger, F. Chemical Interface Damping of Surface Plasmon Excitation in Metal Nanoparticles: A Study by Persistent Spectral Hole Burning. *Appl. Phys. B Lasers Opt.* **2003**, *76*, 869–875.

(20) Chemical Interface Damping in Single Gold Nanorods and Its Near Elimination by Tip-Specific Functionalization - Zijlstra - 2012 - Angewandte Chemie International Edition - Wiley Online Library https://onlinelibrary.wiley.com/doi/abs/10.1002/anie.201202318 (accessed May 29, 2018).

(21) Douglas-Gallardo, O. A.; Berdakin, M.; Sánchez, C. G. Atomistic Insights into Chemical Interface Damping of Surface Plasmon Excitations in Silver Nanoclusters. *J. Phys. Chem. C* **2016**, *120* (42), 24389–24399.

(22) Lermé, J.; Baida, H.; Bonnet, C.; Broyer, M.; Cottancin, E.; Crut, A.; Maioli, P.; Del Fatti, N.; Vallée, F.; Pellarin, M. Size Dependence of the Surface Plasmon Resonance Damping in Metal Nanospheres. *J. Phys. Chem. Lett.* **2010**, *1* (19), 2922–2928.

(23) Voisin, C.; Del Fatti, N.; Christofilos, D.; Vallée, F. Ultrafast Electron Dynamics and Optical Nonlinearities in Metal Nanoparticles. *J. Phys. Chem. B* **2001**, *105* (12), 2264–2280.

(24) Bonn, null; Funk, null; Hess, null; Denzler, null; Stampfl, null; Scheffler, null; Wolf, null; Ertl, null. Phonon- versus Electron-Mediated Desorption and Oxidation of CO on Ru(0001). *Science* **1999**, *285* (5430), 1042–1045.

(25) Selective and sensitive detection of metal ions by plasmonic resonance energy transfer-based nanospectroscopy | Nature Nanotechnology https://www.nature.com/articles/nnano.2009.258 (accessed May 29, 2018).

(26) Catchpole, K. R.; Polman, A. Plasmonic Solar Cells. *Opt. Express* **2008**, *16* (26), 21793–21800.

(27) Mubeen, S.; Hernandez-Sosa, G.; Moses, D.; Lee, J.; Moskovits, M. Plasmonic Photosensitization of a Wide Band Gap Semiconductor: Converting Plasmons to Charge Carriers. *Nano Lett.* **2011**, *11* (12), 5548–5552.

(28) Plasmon Resonant Enhancement of Photocatalytic Water Splitting Under Visible Illumination - Nano Letters (ACS Publications) https://cdn-pubs.acs.org/doi/10.1021/nl104005n (accessed May 29, 2018).

(29) Schatz, G. C.; Young, M. A.; Duyne, R. P. V. Electromagnetic Mechanism of SERS. 28.

(30) Boerigter, C.; Aslam, U.; Linic, S. Mechanism of Charge Transfer from Plasmonic Nanostructures to Chemically Attached Materials. *ACS Nano* **2016**, *10* (6), 6108–6115.

(31) Brown, J. M.; Cooley, N. A. Carbon-Carbon Bond Formation through Organometallic Elimination Reactions. *Chem. Rev.* **1988**, *88* (7), 1031–1046.

(32) Taber, D. Best Synthetic Methods: Carbon-Carbon Bond Formation. *Org. Chem. Highlights* **2007**.

(33) Brahmachari, G. Design of Organic Transformations at Ambient Conditions: Our Sincere Efforts to the Cause of Green Chemistry Practice. *Chem. Rec.* **2018**, *16* (1), 98–123.

(34) T. Ren; Y. Zhang; W. Zhu; J. Zhou. *Synth. Commun. 37*, 3729–3290.

(35) The first Cu- and amine-free Sonogashira-type cross-coupling in the C-6-alkynylation of protected 2′-deoxyadenosine - ScienceDirect https://www.sciencedirect.com/science/article/pii/S0040402009004281 (accessed May 29, 2018).

(36) Sustainable HandaPhos-ppm Palladium Technology for Copper-Free Sonogashira Couplings in Water under Mild Conditions - Organic Letters (ACS Publications) https://pubs.acs.org/doi/abs/10.1021/acs.orglett.7b03621 (accessed May 29, 2018).

(37) Biffis, A.; Scattolin, E.; Ravasio, N.; Zaccheria, F. Supported Copper Precatalysts for Ligand-Free, Palladium-Free Sonogashira Coupling Reactions. *Tetrahedron Lett.* **2007**, *48* (49), 8761–8764.

(38) Thathagar, M. B.; Beckers, J.; Rothenberg, G. Palladium-Free and Ligand-Free Sonogashira Cross-Coupling. *Green Chem.* **2004**, *6* (4), 215–218.

(39) Fleischmann, M.; Hendra, P. J.; McQuillan, A. J. Raman Spectra of Pyridine Adsorbed at a Silver Electrode. *Chem. Phys. Lett.* **1974**, *26* (2), 163–166.

(40) *Practical Raman Spectroscopy*; Gardiner, D. J., Graves, P. R., Eds.; Springer-Verlag: Berlin Heidelberg, 1989.

(41) Moskovits, M.; Tay, L.-L.; Yang, J.; Haslett, T. SERS and the Single Molecule. In *Optical Properties of Nanostructured Random Media*; Topics in Applied Physics; Springer, Berlin, Heidelberg, 2002; pp 215–227.

(42) Willets, K. A.; Van Duyne, R. P. Localized Surface Plasmon Resonance Spectroscopy and Sensing. *Annu. Rev. Phys. Chem.* **2007**, *58*, 267–297.

(43) Mock, J. J.; Barbic, M.; Smith, D. R.; Schultz, D. A.; Schultz, S. Shape Effects in Plasmon Resonance of Individual Colloidal Silver Nanoparticles. *J. Chem. Phys.* **2002**, *116* (15), 6755–6759.

(44) Agnihotri, S.; Mukherji, S.; Mukherji, S. Size-Controlled Silver Nanoparticles Synthesized over the Range 5–100 Nm Using the Same Protocol and Their Antibacterial Efficacy. *RSC Adv.* **2013**, *4* (8), 3974–3983.

(45) Amendola, V.; Meneghetti, M. Size Evaluation of Gold Nanoparticles by UV−vis Spectroscopy. *J. Phys. Chem. C* **2009**, *113* (11), 4277–4285.

(46) Ma, X.-C.; Dai, Y.; Yu, L.; Huang, B.-B. Energy Transfer in Plasmonic Photocatalytic Composites. *Light Sci. Appl.* **2016**, *5* (2), e16017.

(47) Attia, Y. A.; Buceta, D.; Requejo, F. G.; Giovanetti, L. J.; López-Quintela, M. A. Photostability of Gold Nanoparticles with Different Shapes: The Role of Ag Clusters. *Nanoscale* **2015**, *7* (26), 11273–11279.

(48) Kong, K. V.; Ho, C. J. H.; Gong, T.; Lau, W. K. O.; Olivo, M. Sensitive SERS Glucose Sensing in Biological Media Using Alkyne Functionalized Boronic Acid on Planar Substrates. *Biosens. Bioelectron.* **2014**, *56*, 186–191.

(49) Wang, A.; Huang, Y.-F.; Sur, U. K.; Wu, D.-Y.; Ren, B.; Rondinini, S.; Amatore, C.; Tian, Z.-Q. In Situ Identification of Intermediates of Benzyl Chloride Reduction at a Silver Electrode by SERS Coupled with DFT Calculations. *J. Am. Chem. Soc.* **2010**, *132* (28), 9534–9536.

(50) Saha, K.; Agasti, S. S.; Kim, C.; Li, X.; Rotello, V. M. Gold Nanoparticles in Chemical and Biological Sensing. *Chem. Rev.* **2012**, *112* (5), 2739–2779.

(51) Lu, X.; Rycenga, M.; Skrabalak, S. E.; Wiley, B.; Xia, Y. Chemical Synthesis of Novel Plasmonic Nanoparticles. *Annu. Rev. Phys. Chem.* **2009**, *60*, 167–192.

(52) Linic, S.; Christopher, P.; Ingram, D. B. Plasmonic-Metal Nanostructures for Efficient Conversion of Solar to Chemical Energy. *Nat. Mater.* **2011**, *10* (12), 911–921.

(53) Watanabe, K.; Menzel, D.; Nilius, N.; Freund, H.-J. Photochemistry on Metal Nanoparticles. *Chem. Rev.* **2006**, *106* (10), 4301–4320.

(54) Ingram, D. B.; Linic, S. Water Splitting on Composite Plasmonic-Metal/Semiconductor Photoelectrodes: Evidence for Selective Plasmon-Induced Formation of Charge Carriers near the Semiconductor Surface. *J. Am. Chem. Soc.* **2011**, *133* (14), 5202–5205.

(55) Zhou, X.; Liu, G.; Yu, J.; Fan, W. Surface Plasmon Resonance-Mediated Photocatalysis by Noble Metal-Based Composites under Visible Light. *J. Mater. Chem.* **2012**, *22* (40), 21337–21354.

(56) Baijoli, A.; S., C.; Limberger, J.; Claudino, T.; Monteiro, A. J. *J. Braz. Chem. Soc.* **2014**, *25* (12), 91501–91970.

(57) Sonogashira, K. Development of Pd–Cu Catalyzed Cross-Coupling of Terminal Acetylenes with Sp2-Carbon Halides. *J. Organomet. Chem.* **2002**, *653* (1), 46–49.

(58) Evano, G.; Blanchard, N.; Toumi, M. Copper-Mediated Coupling Reactions and Their Applications in Natural Products and Designed Biomolecules Synthesis. *Chem. Rev.* **2008**, *108* (8), 3054–3131.

(59) Das, S.; Samanta, S.; Ray, S.; Biswas, P. 3,6-Di(Pyridin-2-Yl)-1,2,4,5-Tetrazine Capped Pd(0) Nanoparticles: A Catalyst for Copper-Free Sonogashira Coupling of Aryl Halides in Aqueous Medium. *RSC Adv.* **2015**, *5* (92), 75263–75267.

(60) Kosugi, M.; Kameyama, M.; Migita, T. Palladium-Catalyzed Aromatic Amination of Aryl Bromides with n,n-Di-Ethylamino-Tributyltin. *Chem. Lett.* **1983**, *12* (6), 927–928.

(61) Galardon, E.; Ramdeehul, S.; Brown, J. M.; Cowley, A.; Hii, K. K. (Mimi); Jutand, A. Profound Steric Control of Reactivity in Aryl Halide Addition to Bisphosphane Palladium(0) Complexes. *Angew. Chem. Int. Ed. 41* (10), 1760–1763.

(62) Heiden, M. an der; Plenio, H. The Effect of Steric Bulk in Sonogashira Coupling Reactions. *Chem. Commun.* **2007**, *0* (9), 972–974.

(63) Tolman, C. A. Steric Effects of Phosphorus Ligands in Organometallic Chemistry and Homogeneous Catalysis. *Chem. Rev.* **1977**, *77* (3), 313–348.

(64) Imura, Y.; Shimojuh, N.; Kawano, Y.; Togo, H. Novel Preparation of Ion-Supported Triphenylphosphines and Their Synthetic Utility. *Tetrahedron* **2010**, *66* (19), 3421–3426.

(65) Fleckenstein, C. A.; Plenio, H. 9-Fluorenylphosphines for the Pd-Catalyzed Sonogashira, Suzuki, and Buchwald–Hartwig Coupling Reactions in Organic Solvents and Water. *Chem. – Eur. J. 13* (9), 2701–2716.

(66) Astruc, D. Palladium Nanoparticles as Efficient Green Homogeneous and Heterogeneous Carbon−Carbon Coupling Precatalysts: A Unifying View. *Inorg. Chem.* **2007**, *46* (6), 1884–1894.

(67) Gaikwad, A. V.; Holuigue, A.; Thathagar, M. B.; ten Elshof, J. E.; Rothenberg, G. Ion- and Atom-Leaching Mechanisms from Palladium Nanoparticles in Cross-Coupling Reactions. *Chem. – Eur. J. 13* (24), 6908–6913.

(68) Widegren, J. A.; Finke, R. G. A Review of the Problem of Distinguishing True Homogeneous Catalysis from Soluble or Other Metal-Particle Heterogeneous Catalysis under Reducing Conditions. *J. Mol. Catal. Chem.* **2003**, *198* (1), 317–341.

(69) Li, H.; Zhu, Z.; Li, H.; Li, P.; Zhou, X. Recyclable Hollow Pd-Fe Nanospheric Catalyst for Sonogashira-, Heck-, and Ullmann-Type Coupling Reactions of Aryl Halide in Aqueous Media. *J. Colloid Interface Sci.* **2010**, *349* (2), 613–619.

(70) Jiang, J.-Z.; Cai, C. Copper- and Ligand-Free Sonogashira Reaction Catalyzed by Palladium in Microemulsion. *J. Colloid Interface Sci.* **2007**, *307* (1), 300–303.

(71) Sawoo, S.; Srimani, D.; Dutta, P.; Lahiri, R.; Sarkar, A. Size Controlled Synthesis of Pd Nanoparticles in Water and Their Catalytic Application in C–C Coupling Reactions. *Tetrahedron* **2009**, *65* (22), 4367–4374.

(72) Pandey, P. C.; Singh, R.; Pandey, A. K. Tetrahydrofuran Hydroperoxide and 3-Aminopropyltrimethoxysilane Mediated Controlled Synthesis of Pd, Pd-Au, Au-Pd Nanoparticles: Role of Palladium Nanoparticles on the Redox Electrochemistry of Ferrocene Monocarboxylic Acid. *Electrochimica Acta* **2014**, *138*, 163–173.

(73) Zhao, J.; Pinchuk, A. O.; McMahon, J. M.; Li, S.; Ausman, L. K.; Atkinson, A. L.; Schatz, G. C. Methods for Describing the Electromagnetic Properties of Silver and Gold Nanoparticles. *Acc. Chem. Res.* **2008**, *41* (12), 1710–1720.

(74) Handbook of Optical Constants of Solids - 1st Edition https://www.elsevier.com/books/handbook-of-optical-constants-of-solids/palik/978-0-08-055630-7 (accessed May 30, 2018).

(75) Vaughan, O. P. H.; Kyriakou, G.; Macleod, N.; Tikhov, M.; Lambert, R. M. Copper as a Selective Catalyst for the Epoxidation of Propene. *J. Catal.* **2005**, *236* (2), 401–404.

(76) Linic, S.; Christopher, P.; Ingram, D. B. Plasmonic-Metal Nanostructures for Efficient Conversion of Solar to Chemical Energy. *Nat. Mater.* **2011**, *10* (12), 911–921.

(77) Elias, W. C.; Signori, A. M.; Zaramello, L.; Albuquerque, B. L.; de Oliveira, D. C.; Domingos, J. B. Mechanism of a Suzuki-Type Homocoupling Reaction Catalyzed by Palladium Nanocubes. *ACS Catal.* **2017**, *7* (2), 1462–1469.

(78) Beletskaya, I. P.; Cheprakov, A. V. Copper in Cross-Coupling Reactions: The Post-Ullmann Chemistry. *Coord. Chem. Rev.* **2004**, *248* (21), 2337–2364.

(79) Kyriakou, G.; Beaumont, S. K.; Humphrey, S. M.; Antonetti, C.; Lambert, R. M. Sonogashira Coupling Catalyzed by Gold Nanoparticles: Does Homogeneous or Heterogeneous Catalysis Dominate? *ChemCatChem* **2010**, *2* (11), 1444–1449.

(80) Sarvi, I.; Gholizadeh, M.; Izadyar, M. Highly Dispersed Palladium Nanoparticle-Loaded Magnetic Catalyst (FeS@EP–AG–Pd) for Suzuki Reaction in Water. *Catal. Lett.* **2017**, *147* (5), 1162–1171.

(81) Mohammadparasat, F.; Dadgar, A.; Tirumala, R. T. A.; Mohammad, S.; Topal, O.; Kalkan, K.; Andiappan, M. Localized Surface Plasmon Resonance Spectroscopy as Platform for Characterization of Metal Nanoparticle Catalyzed Coupling Reactions. *Submitted, Manuscript I.D. : ja-2018-07232m*

(82) Jana, N. R.; Gearheart, L.; Murphy, C. J. Seeding Growth for Size Control of 5−40 Nm Diameter Gold Nanoparticles. *Langmuir* **2001**, *17* (22), 6782–6786.

(83) Kooti, M. Fabrication of Nanosized Cuprous Oxide Using Fehling's Solution. *Trans. F Nanotechnol.* **2010**, *17*, 73.

(84) Narushima, T.; Tsukamoto, H.; Yonezawa, T. High Temperature Oxidation Event of Gelatin Nanoskin-Coated Copper Fine Particles Observed by in Situ TEM. *AIP Adv.* **2012**, *2*.

(85) Bardhan, R.; Mukherjee, S.; Mirin, N. A.; Levit, S. D.; Nordlander, P.; Halas, N. J. Nanosphere-in-a-Nanoshell: A Simple Nanomatryushka. *J. Phys. Chem. C* **2010**, *114* (16), 7378–7383.

(86) Jain, P. K.; El-Sayed, M. A. Universal Scaling of Plasmon Coupling in Metal Nanostructures: Extension from Particle Pairs to Nanoshells. *Nano Lett.* **2007**, *7* (9), 2854–2858.

(87) Radloff, C.; Halas, N. J. Plasmonic Properties of Concentric Nanoshells. *Nano Lett.* **2004**, *4* (7), 1323–1327.

(88) Mohammadparasat, F.; Dadgar, A.; Topal, O.; Kalkan, K.; Andiappan, M. Investigation of Energy Transfer Pathways in Cu/Cu2O Nanostructures. *In Preparation*

(89) Hövel, H.; Fritz, S.; Hilger, A.; Kreibig, U.; Vollmer, M. Width of Cluster Plasmon Resonances: Bulk Dielectric Functions and Chemical Interface Damping. *Phys. Rev. B* **1993**, *48* (24), 18178–18188.

(90) Mehrdel, B.; Aziz, A. A.; Yoon, T. L.; Lee, S. C. Effect of Chemical Interface Damping and Aggregation Size of Bare Gold Nanoparticles in NaCl on the Plasmon Resonance Damping. *Opt. Mater. Express* **2017**, *7* (3), 955–966.

(91) Palik, E. D. *Handbook of Optical Constants of Solids*, 1 edition.; Academic Press: San Diego, Calif., 1997.

(92) Tirumala, R. T. A.; Dadgar, A.; Mohammadparasat, F.; Andiappan, M. Copper Nanoparticle Catalyzed Sonogashira Coupling. *In Preparation*

(93) Panova, Y. S.; Kashin, A. S.; Vorobev, M. G.; Degtyareva, E. S.; Ananikov, V. P. Nature of the Copper-Oxide-Mediated C–S Cross-Coupling Reaction: Leaching of Catalytically Active Species from the Metal Oxide Surface. *ACS Catal.* **2016**, *6* (6), 3637–3643.

(94) Barbon, S. M.; Staroverov, V. N.; Gilroy, J. B. Effect of Extended π Conjugation on the Spectroscopic and Electrochemical Properties of Boron Difluoride Formazanate Complexes. *J. Org. Chem.* **2015**, *80* (10), 5226–5235.

(95) Li, Y.; Dandu, N.; Liu, R.; Li, Z.; Kilina, S.; Sun, W. Effects of Extended π-Conjugation in Phenanthroline (N∧N) and Phenylpyridine (C∧N) Ligands on the Photophysics and Reverse Saturable Absorption of Cationic Heteroleptic Iridium(III) Complexes. *J. Phys. Chem. C* **2014**, *118* (12), 6372–6384.

(96) Garcia, M. H.; Mendes, P. J.; Robalo, M. P.; Dias, A. R.; Campo, J.; Wenseleers, W.; Goovaerts, E. Compromise between Conjugation Length and Charge-Transfer in Nonlinear Optical H5-Monocyclopentadienyliron(II) Complexes with Substituted Oligo-Thiophene Nitrile Ligands: Synthesis, Electrochemical Studies and First Hyperpolarizabilities. *J. Organomet. Chem.* **2007**, *692* (14), 3027–3041.

(97) Jana, N. R.; Gearheart, L.; Murphy, C. J. Seeding Growth for Size Control of 5−40 Nm Diameter Gold Nanoparticles. *Langmuir* **2001**, *17* (22), 6782–6786.

APPENDICES

Preparation of Au nanocatalyst

The procedure used for synthesis of Au nanospheres was adapted from Jana et al.[97] First the growth solution was prepared by adding 52 mg of HAuCl * 3 H_2O to 20 mL water. This solution was then added to 300 mL of water. 50 mL of water was used to wash the gold solution into the 300 mL solution. Next 6 grams of cetyltrimethylammonium bromide (CTAB) was added to the solution. The solution while stirring was then heated to 70˚C. In order to make seeds, 180 mL of the growth solution was split aside. To this second solution, a stock solution of 15 mg of sodium citrate in 20 mL of water was added first followed by 24 mg of sodium borohydride in 6 mL of water at 40˚F. This seed solution was then stirred for 1 hour at room temperature to allow seed particles to grow. The final seed size was approximately 3 nm. The first growth step is taken after an hour by adding 18 mL of the growth solution to 0.1 mL of ascorbic acid stock solution prepared by adding 88 mg into 5 mL of water. Then 2 mL of seed solution prepared before is added to the mixture and stirred for 15 min. This yielded Au nanospheres of approximately 7 nm diameter. In order to make large particles, 180 mL of growth solution is stirred with additions of 1 mL ascorbic acid stock solution and the small particle solution prepared before. This solution is stirred at room temperature for 1.5 hours. After the particles were grown, the solution was chilled to 0˚C in order to crystallize CTAB. The solution was then centrifuged at low temperatures to settle out the CTAB crystals. The liquid nanoparticle solution was then transferred to a rotary evaporator to concentrate the solution for use in reactions. The evaporation conditions were set at 60 rpm, a vacuum of 300 mmHg, and a bath temperature of 95˚C. This allows for good concentration without excessive aggregation of the particles. The solution was evaporated until 120 mL is left. This solution was used for catalyzing coupling reaction.

Procedure for coupling reaction

120 mL of Au nanoparticle solution was added to 24 mL of DMF. The reaction mixture was 83%/17% v/v mixture of water/DMF. The reactant used for this reaction was 2 mL of phenylacetylene (18.2 mmol). 2 grams of potassium carbonate was used as base. The solution was heated to 85˚C while stirring in a round bottom flask. Phenylacetylene and base were added once the solution reaches 85˚C. The reaction was carried out on a magnetic hot plate with an aluminum reaction block around a 200 mL 3 necked round bottom flask. To control temperature, a thermocouple was connected to the hot plate and submerged in the reactor. The middle neck was fitted with a west condenser to catch any vapors generated during the reaction. To predict the size of Au nanoparticles as a function of reaction time, the samples for UV-Vis spectra were taken at

frequent time intervals. The UV-Vis extinction spectra were acquired using a Cary 60 spectrophotometer with a Xeon lamp.

Characterization of Au nanoparticles and reaction solution

TEM images were taken using JEOL JEM-2100. The system is equipped with a LaB6 gun and accelerating voltage of 200 kV. Samples were prepared by taking 100uL of growth or reaction mixture and diluting into 2 mL of 200 proof ethanol. This dilution solution was sonicated to ensure good dispersion. Next 10 µL was taken and placed onto a copper mesh carbon background TEM grid. The ethanol was allowed to evaporate at room temperature.

All UV-Vis spectra were taken using an Agilent Cary 60 Spectrophotometer. In operando measurements were taken using a dip probe accessory and a fiber optic coupler with a stainless steel tip. The in operando measurements were taken during growth of Au nanospheres at room temperature in aqueous solution. The data sampled for all Au growth measurements was from 800-300 nm with sampling every 0.5 nm and a scan speed of 300 nm/min. For sampled UV-Vis measurements, 100 uL was taken from the reaction mixture and diluted into 10 mL of 200 proof ethanol. This diluted sample was then used for UV-Vis spectra. A baseline of water was taken prior to running of samples to remove any background contribution from water or the cuvette.

The reaction solution was characterized by GC-MS and HR-ESI-MS. GC-MS samples were prepared by diluting 100 uL of the reaction mixture into 10 mL of dichloromethane. Reaction data was collected on a Shimadzu QP2010SE GC-MS system with helium as the carrier gas with a 5% polar column. HR-ESI-MS spectra for the reaction was collected on a LTQ Orbitrap system with an ESI source. The spray voltage was set at 5.0kV with 15.0 mL/min sample flow rate. The sample was prepared by mixed 1 mL of sample with 1 mL of a mixture of 18 mL DCM, 2 mL Acetone, 400 µL DI water. The sample was sprayed with nitrogen as the sheath and auxiliary gas.

Details of Finite Difference Time Domain (FDTD) simulations

FDTD simulations were used to calculate the extinction cross section for the structures as a function of the incident wavelength. The optical properties for Cu, Au, and Pd were all taken from Palik.[91] The boundary conditions used for the simulations were periodic in the x,y directions and perfectly matched layer (PML) in the z direction. The extinction cross sections as a function of wavelengths were calculated using the total field/scattered-field (TFSF) formalism. The incident light source used for the simulation was Gaussian source in the simulated wavelength region.

Monolayer calculations

For gold and palladium, the parameters used are shown here:
Gold
Structure: FCC
Atomic radii: 0.166 nm
1 monolayer =0.166 x 2 = 0.332 nm

Expected change in particle diameter due to leaching of 1 monolayer of surface atoms = $2 * 0.332\ nm = 0.664\ nm$

1.) Palladium
    a. Structure: FCC
    b. Atomic radii: 0.14 nm
    c. 1 monolayer = 0.14 x 2 = 0.28 nm
    d. Expected change in particle diameter due to leaching of 1 monolayer of surface atoms = $2 * 0.28\ nm = 0.56\ nm$

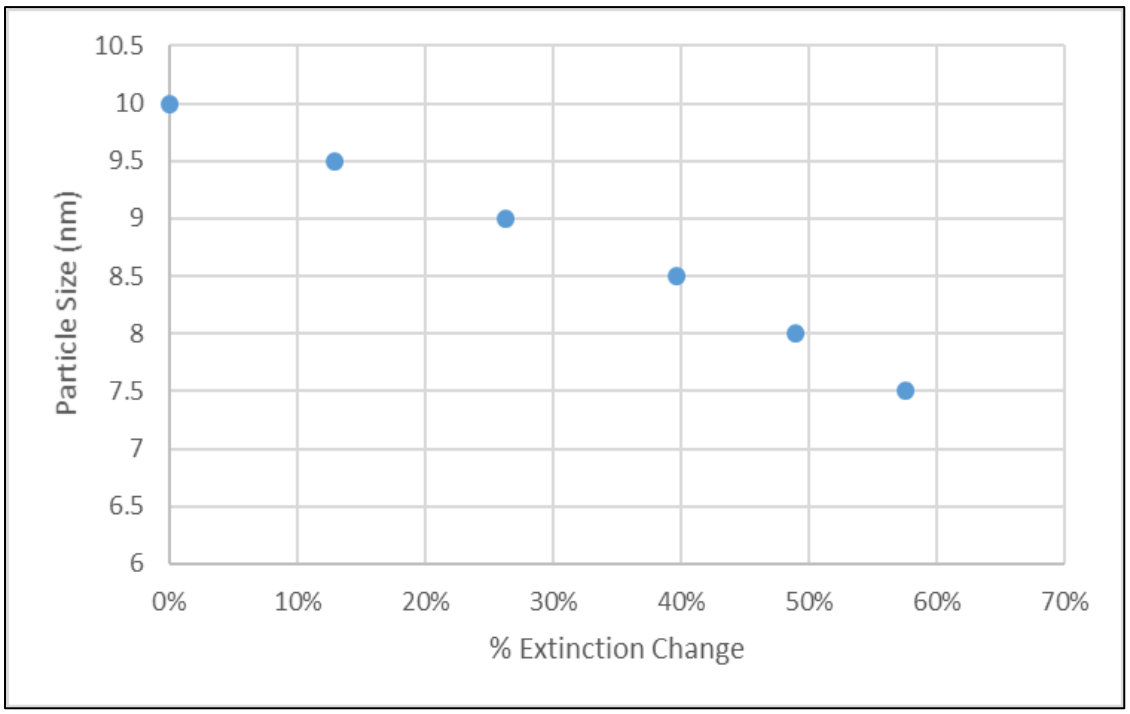

Figure A1.a. Particle size versus % change in extinction for Cu nanospheres at LSPR peak wavelength of ~570 nm.[81]

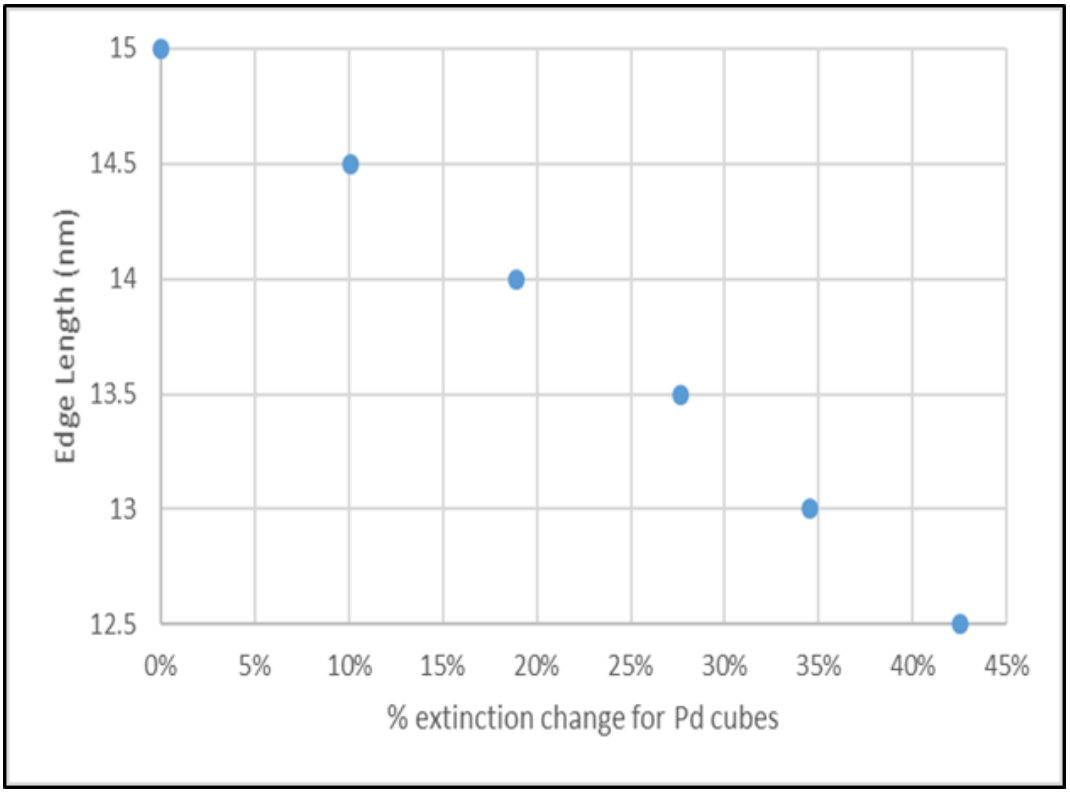

Figure A1.b. Particle size versus % change in extinction for Pd nanocubes at LSPR peak wavelength of ~223 nm.[81]

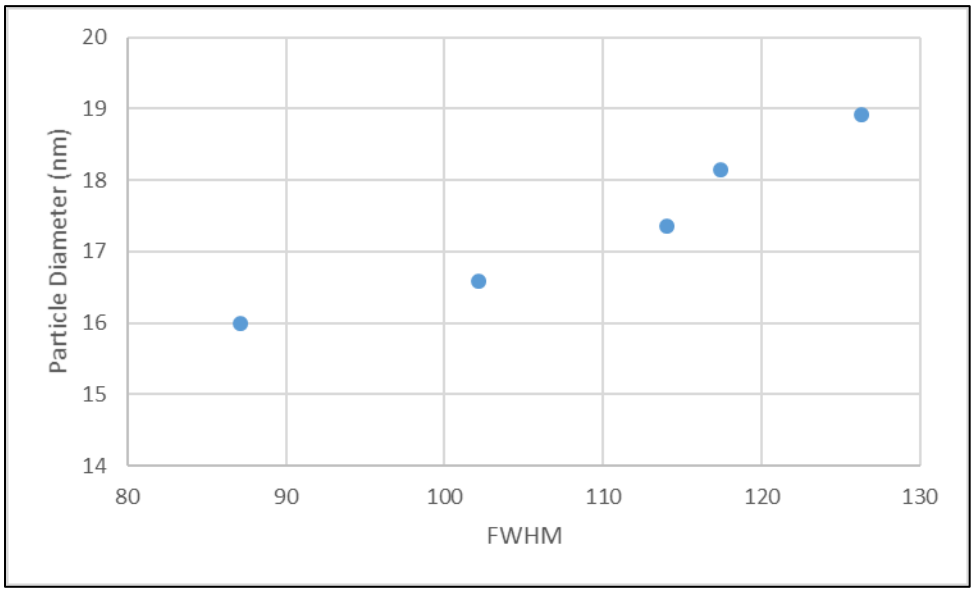

Figure A2.a. Diameter of core-shell Au-Pd nanoparticle as a function FWHM of LSPR peak. The diameter of Au core in core-shell Au-Pd nanoparticle is 16 nm.[81]

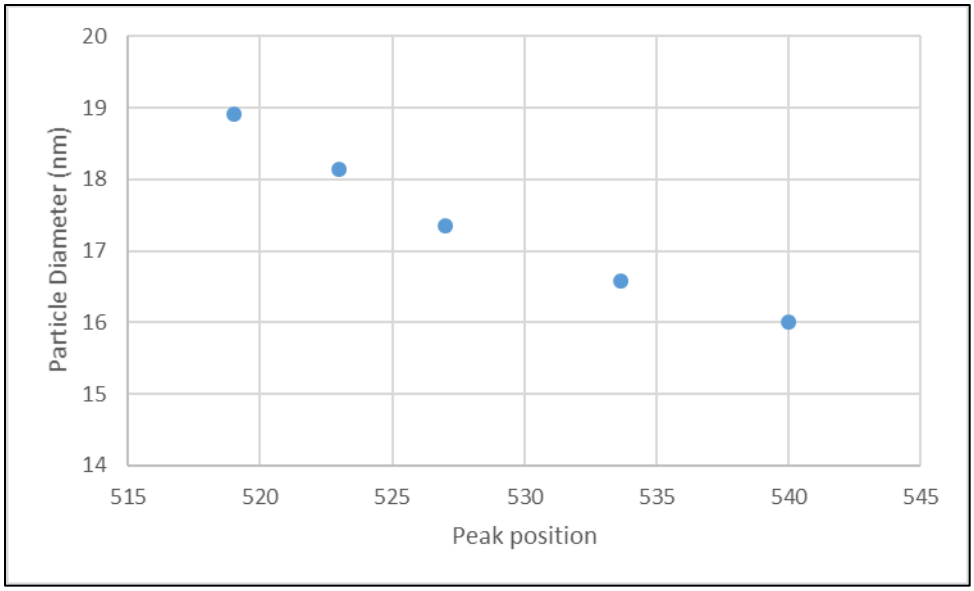

Figure A2.b. Diameter of core-shell Au-Pd nanoparticle as a function of LSPR peak position. The diameter of Au core in core-shell Au-Pd nanoparticle is 16 nm.[81]

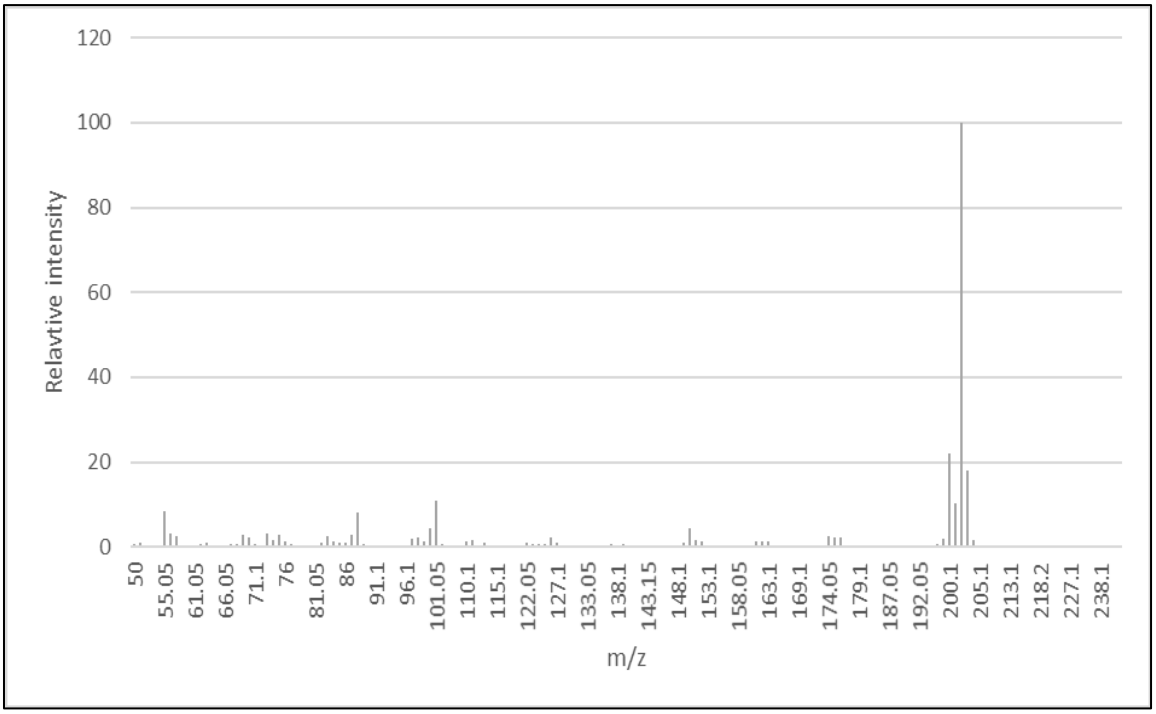

Figure A3. GC-MS (electron ionization) spectrum of diphenyldiacetylene (DPDA) observed in reaction mixture taken from Au nanoparticle catalyzed homo-coupling of phenylacetylene.[81]

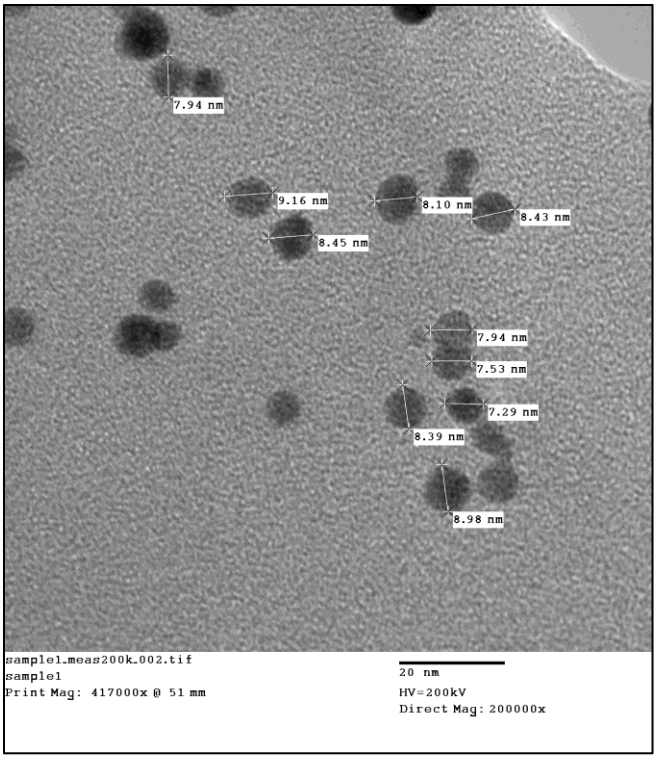

Figure A4. Representative TEM of gold nanoparticles before growth[81]

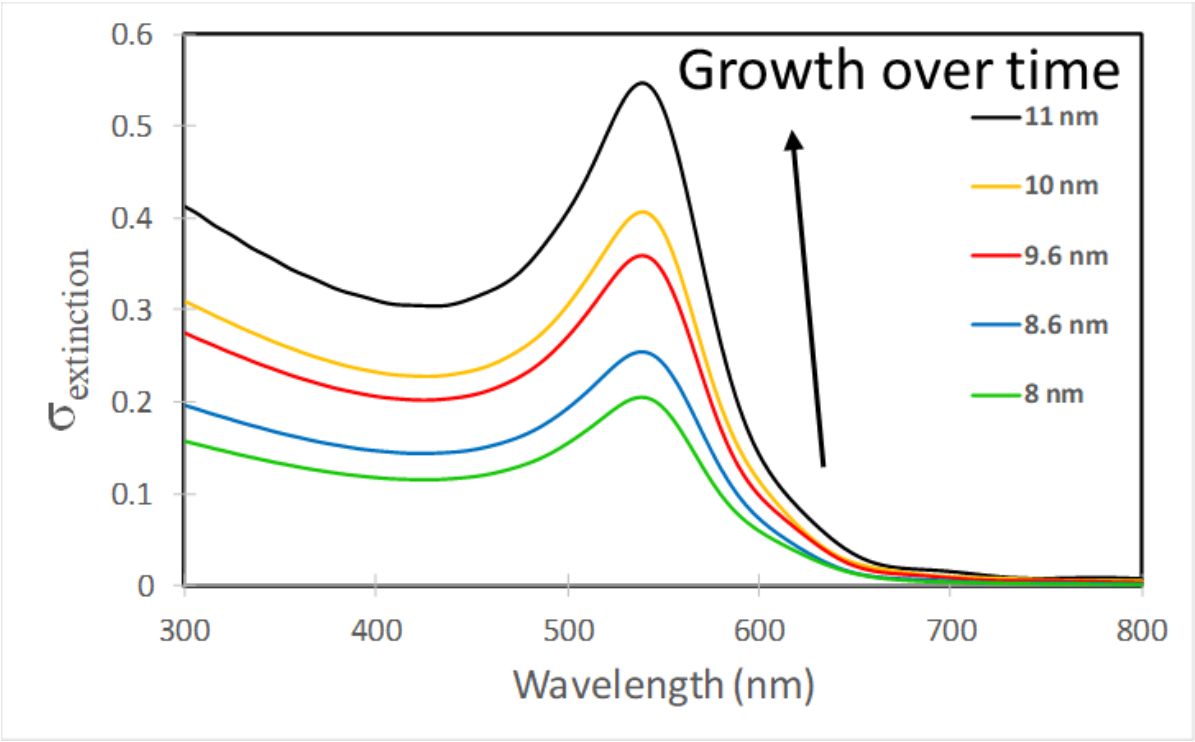

Figure A5. Simulated growth spectra based on TEM sampled particles sizes[81]

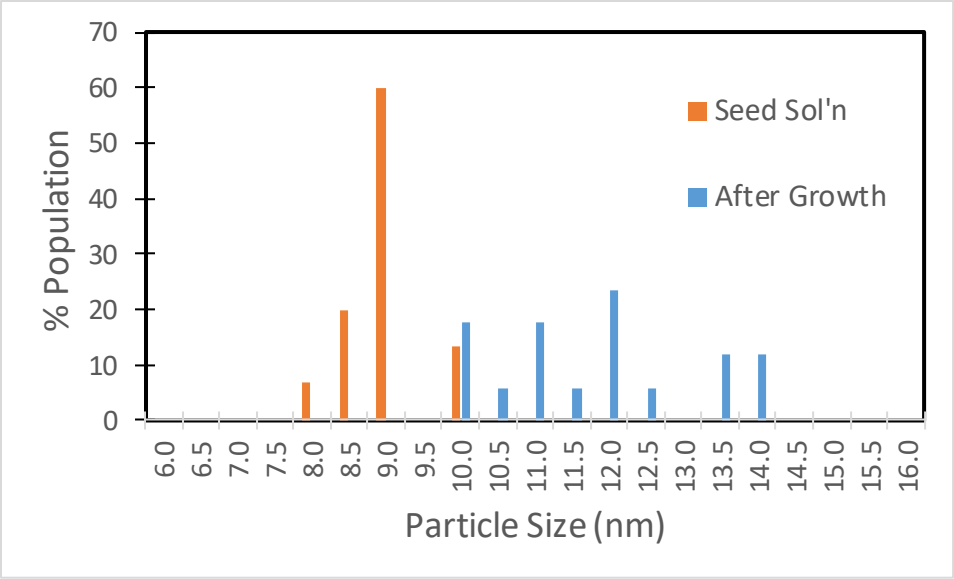

Figure A6. Population distribution of gold particles before and after growth[81]

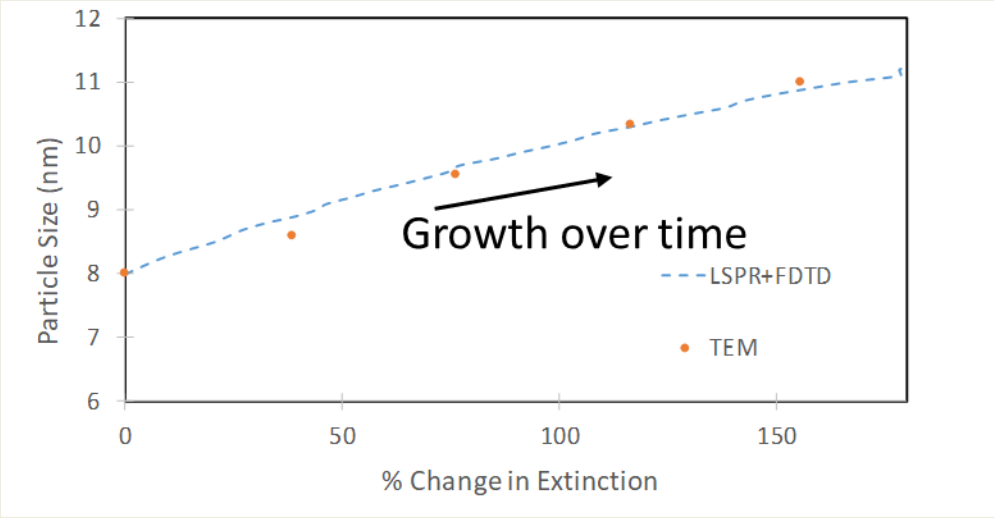

Figure A7. Comparison between simulated (line) and measured (points) particle size vs. the change in the extinction intensity at the LSPR wavelength for gold spheres[81]

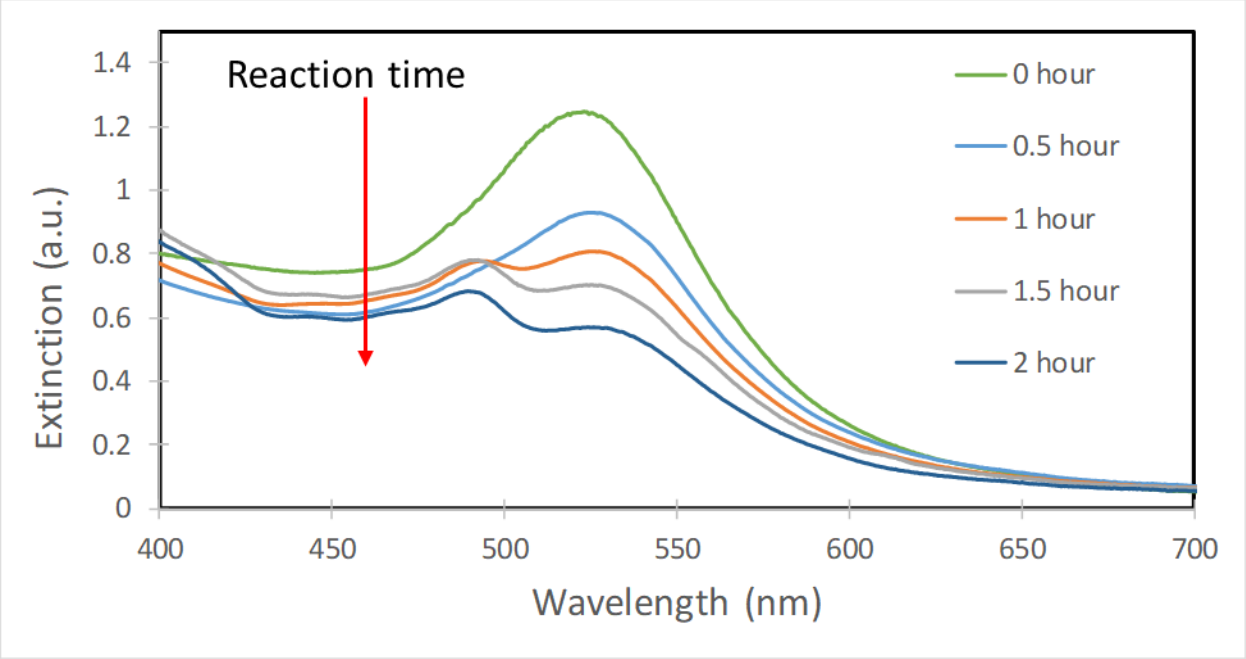

Figure A8. Experimental UV-Vis extinction spectra of gold nanoparticles under oxidative homocoupling conditions taken in operando[81]

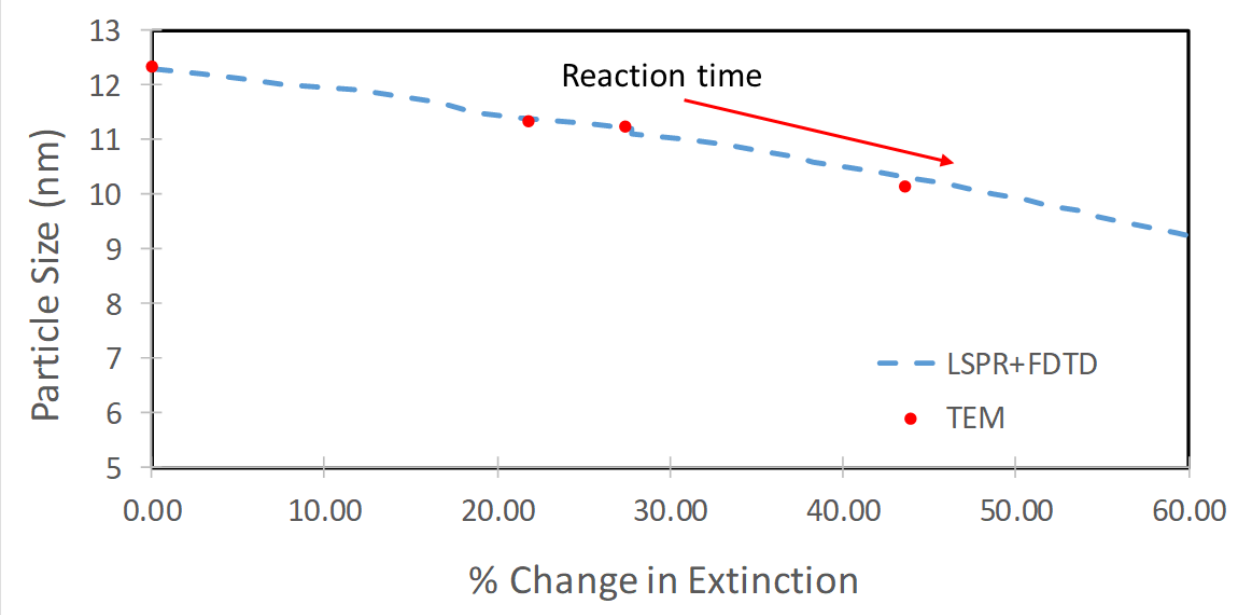

Figure A9. Comparison between simulated (line) and experimental (points) of gold average particle size from oxidative homocoupling of phenylacetylene[81]

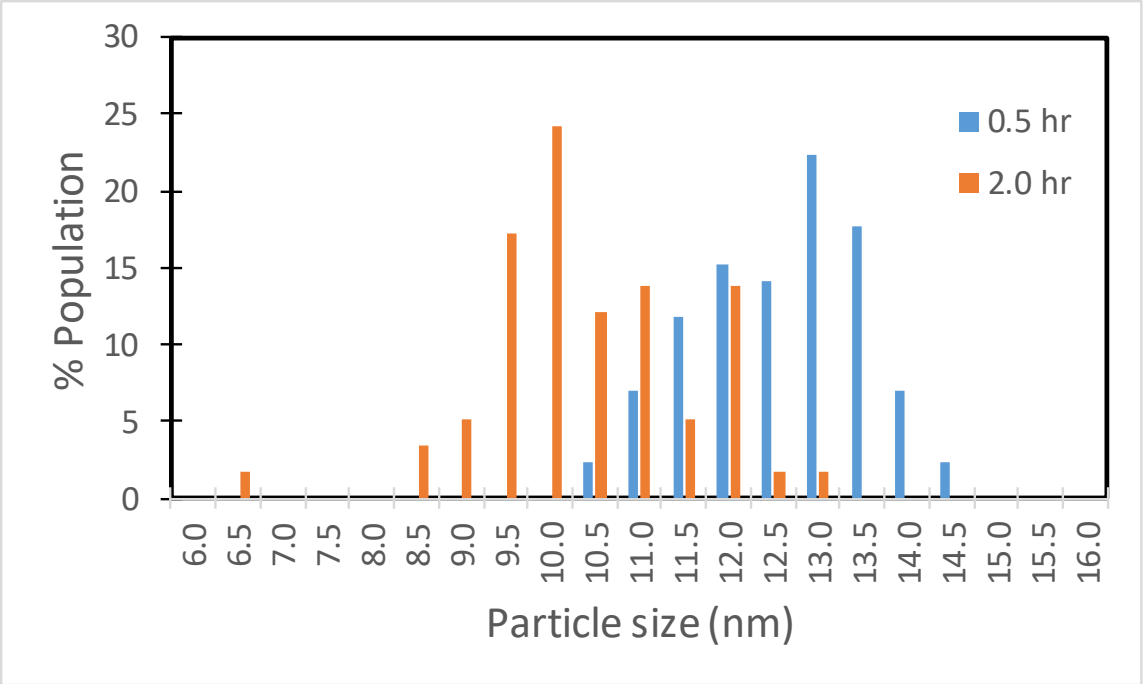

Figure A10. Population distribution of gold particles at half an hour and two hours into oxidative homocoupling of phenylacetylene [81]

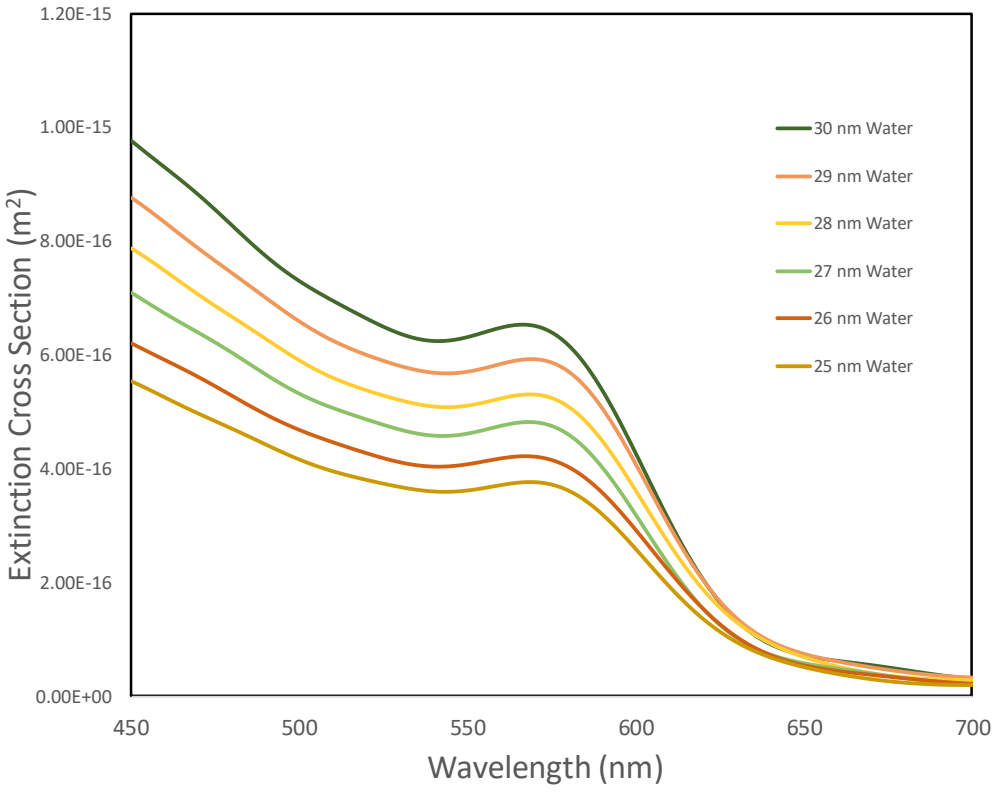

Figure A11. Simulated response of copper spheres in water

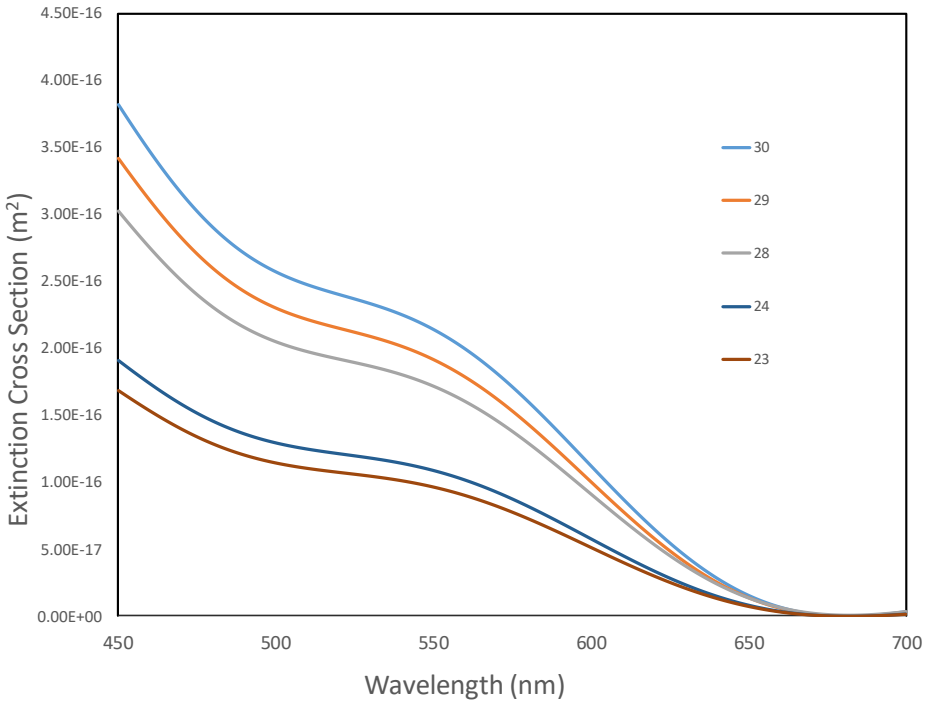

Figure A12. Simulated response of copper spheres in vacuum

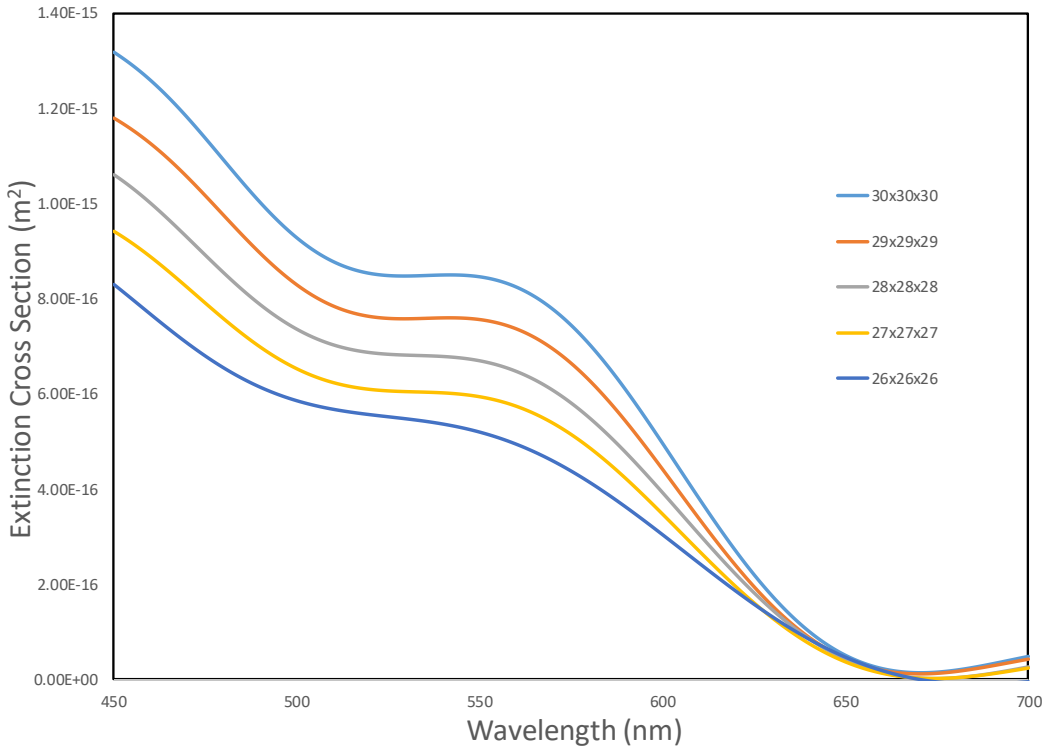

Figure A13. Simulated response of copper cubes in vacuum

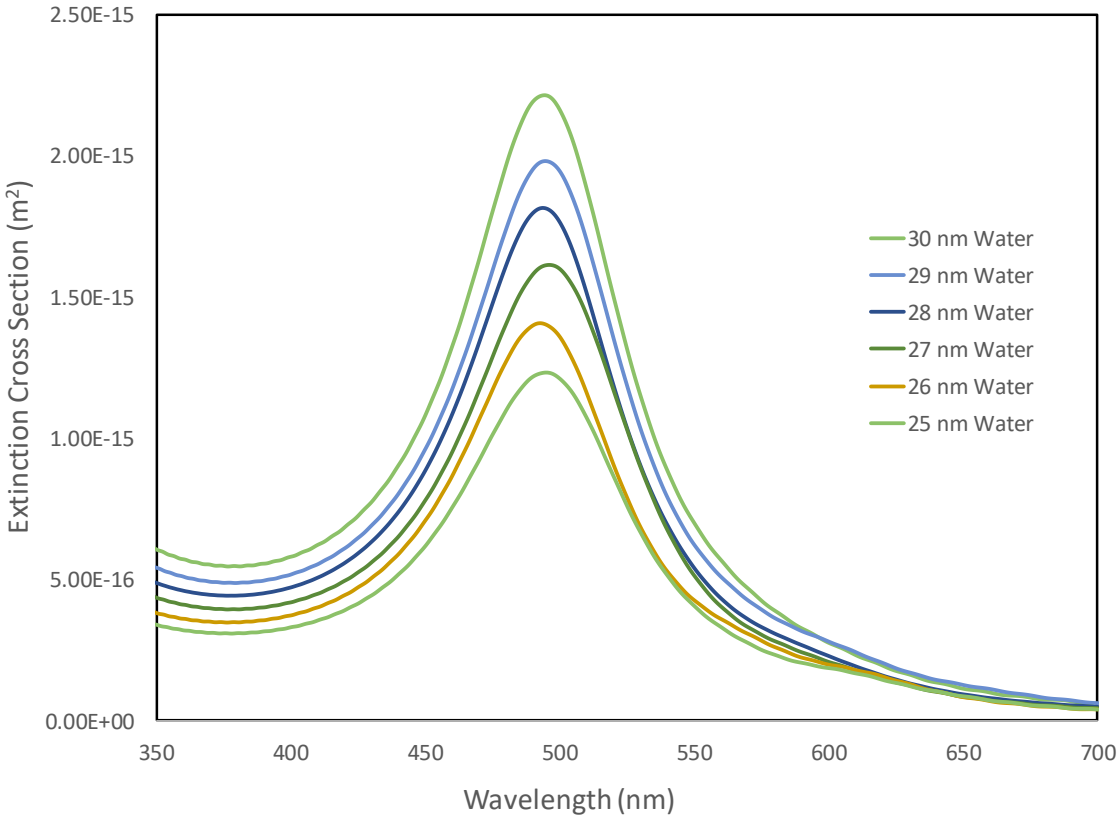

Figure A14. Simulated response for gold spheres in water

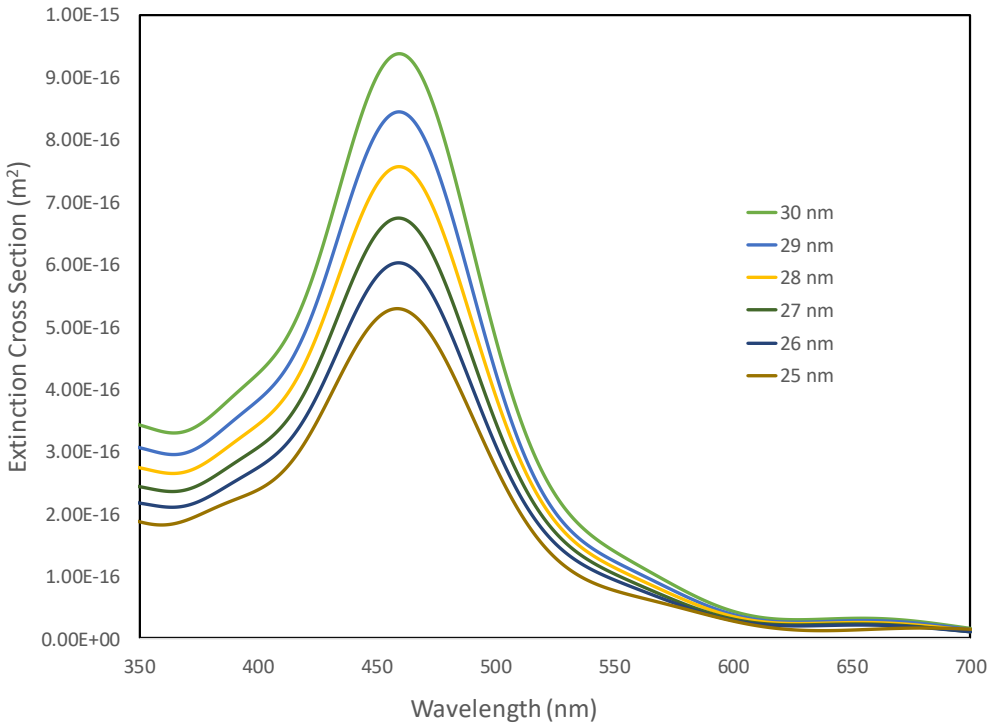

Figure A15. Simulated response of gold spheres in air

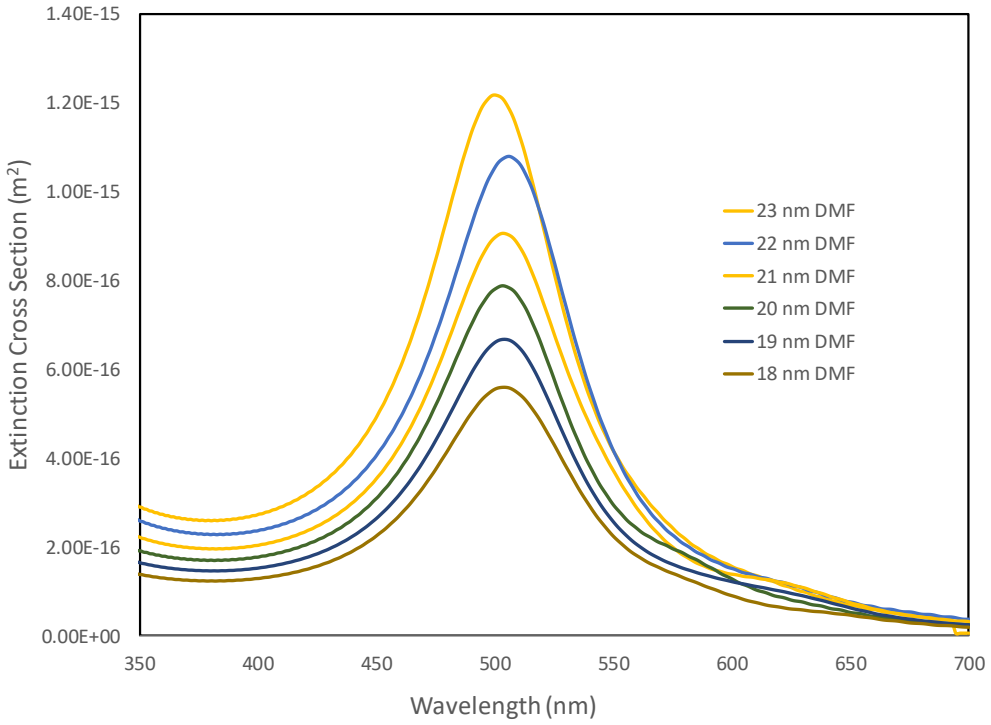

Figure A16. Simulated response of gold spheres in DMF

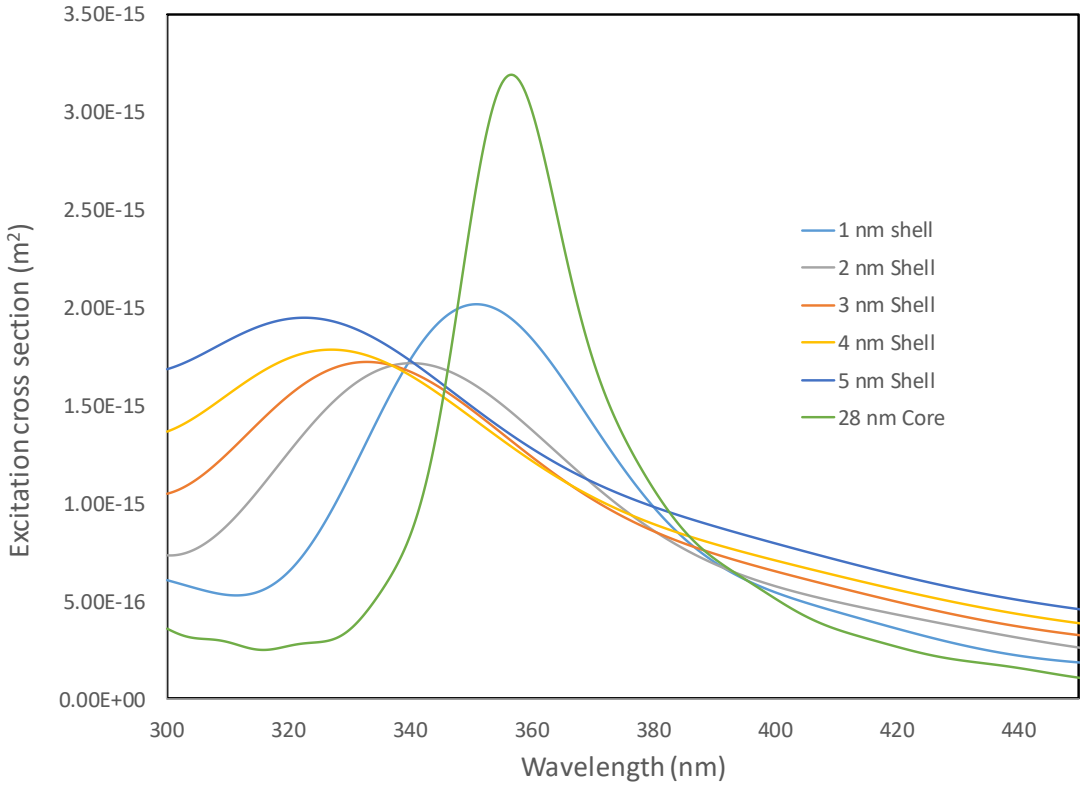

Figure A17. Simulated response of Au-Pd core shell spherical particles in air

Operational Principles and Working Procedure for DRA: For this work a Harrick Scientific diffuse reflectance accessory (DRA) was used to obtain the extinction spectra for supported copper nanoparticles. The unit was coupled with a Cary 60 UV-Vis spectrophotometer. To take measurements, a small number of supported nanoparticles were put onto a glass slide. A second glass slide was used to compress the powder until a uniform surface was seen. This step is critical as the more uneven the surface is, the more noise is present in the measurement. After the sample is pressed, the spacer plate is positioned over a spot. The DRA is then placed into the spacer and rotated to ensure the feet are lined up with the holes in the spacer. The measurement is taken by pressing start in the program. When finished, the DRA is removed and the spacer is lifted and moved to another spot on the sample. This procedure is repeated until at least 3 spectra are taken that show similar trends. The first sample run each time is a silica blank which is prepared the same as before. The silica serves to remove any effect of the substrate in the measurement.

XRD Operation and Working Procedure: In order to characterize the phase composition in Cu_2O/Cu particles I used x-ray powder diffraction. The measurements were performed on a Phillips XRD. The energy was set to 45 kV and 40 mA. The sample was prepared by taking reduced powder and pouring it into a sample holder. The sample was then leveled to the sides of the holder. Any large particles were broken up in order to reduce the noise level. The sample was then placed in the instrument and the doors were closed. The data was taken at 20^o-90^o with a data point taken at every 0.02^o with a collection time of 0.5 seconds per point. After the spectra was taken the sample was returned to the vial for further processing. No color change was observed during the measurements indicating that oxidation did not happen during the measurement.

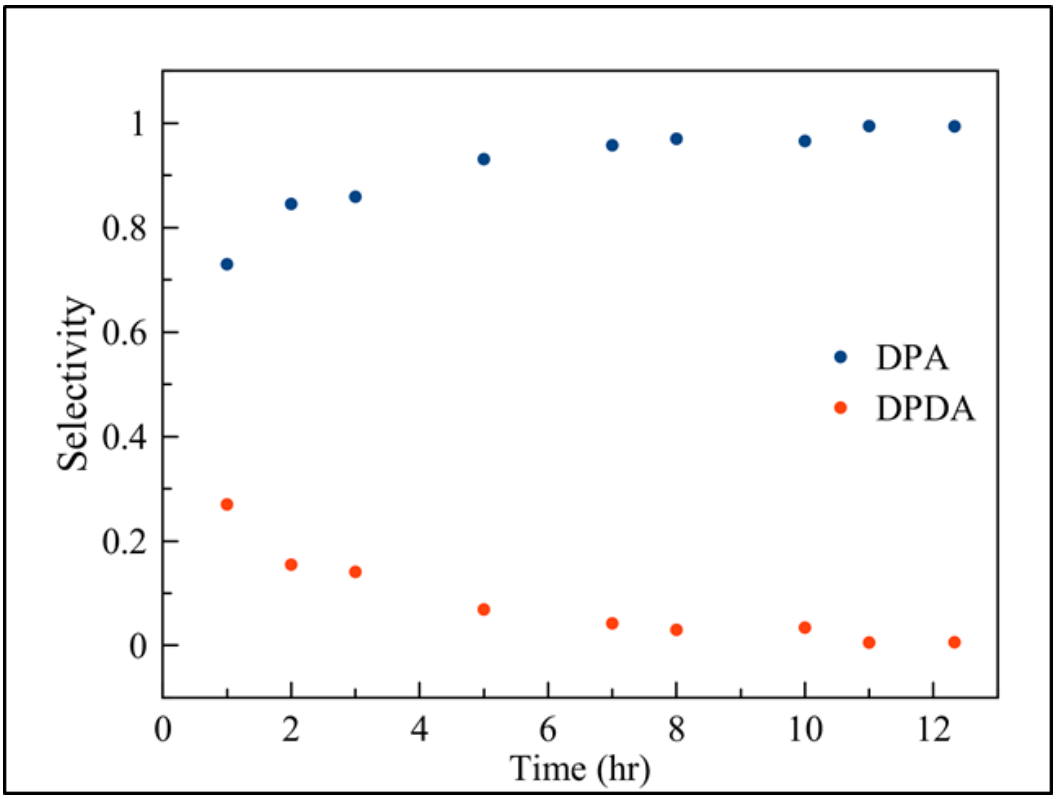

Figure A18 Selectivity of DPA and DPDA versus reaction time for heterocoupling of PA and IB under reflux in DMF with base and N_2 blanket[92]

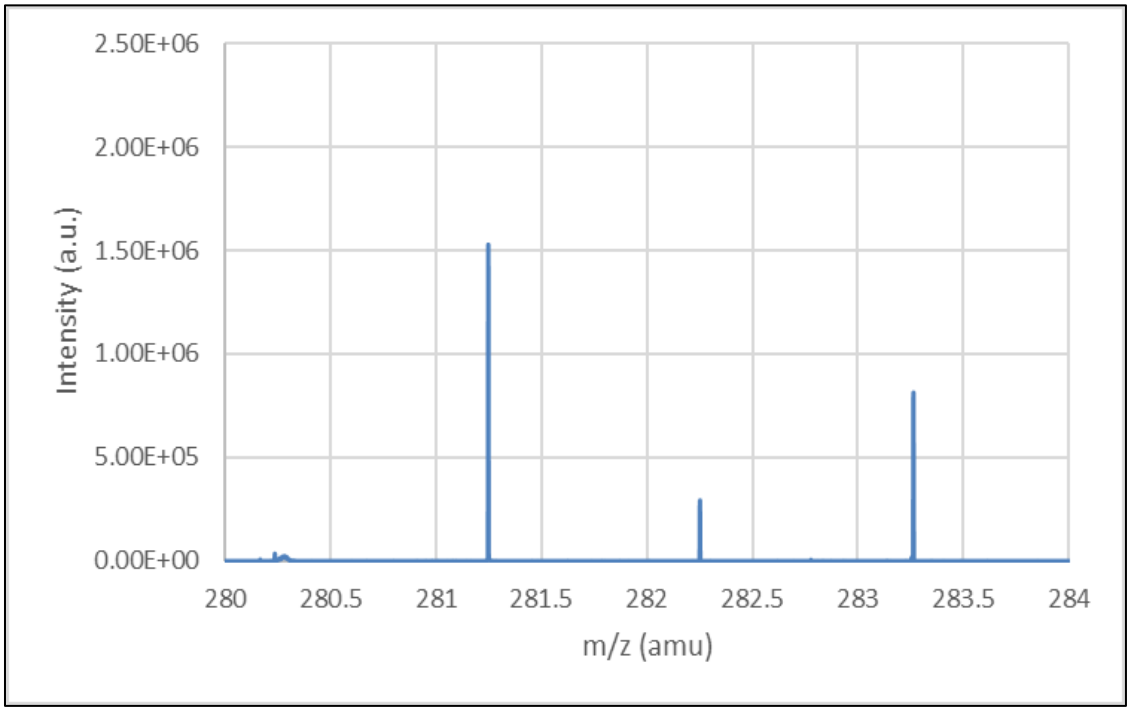

Figure A19 ESI-MS spectra for 281.26/283.26 from Experiment 1-148-3

EI for PA, IB, DPA

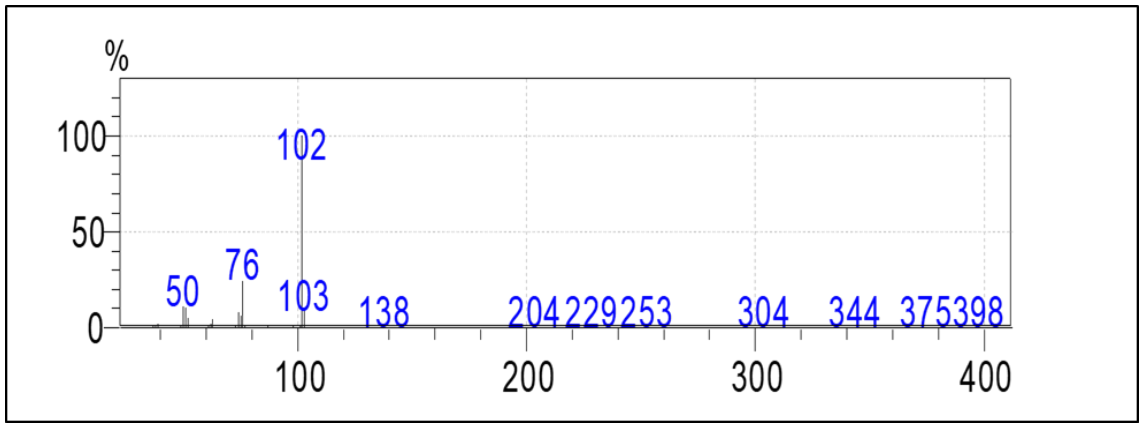

Figure A20 Experimental EI spectra for PA NIST ref:
https://webbook.nist.gov/cgi/cbook.cgi?ID=C536743&Mask=200#Mass-Spec

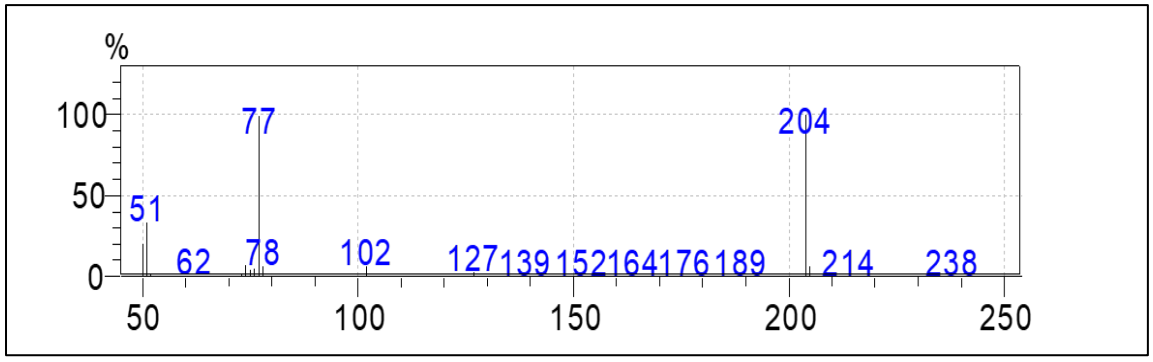

Figure A21 Experimental EI spectra for Iodobenzene NIST Ref:
https://webbook.nist.gov/cgi/cbook.cgi?ID=C591504&Units=SI&Mask=200#Mass-Spec

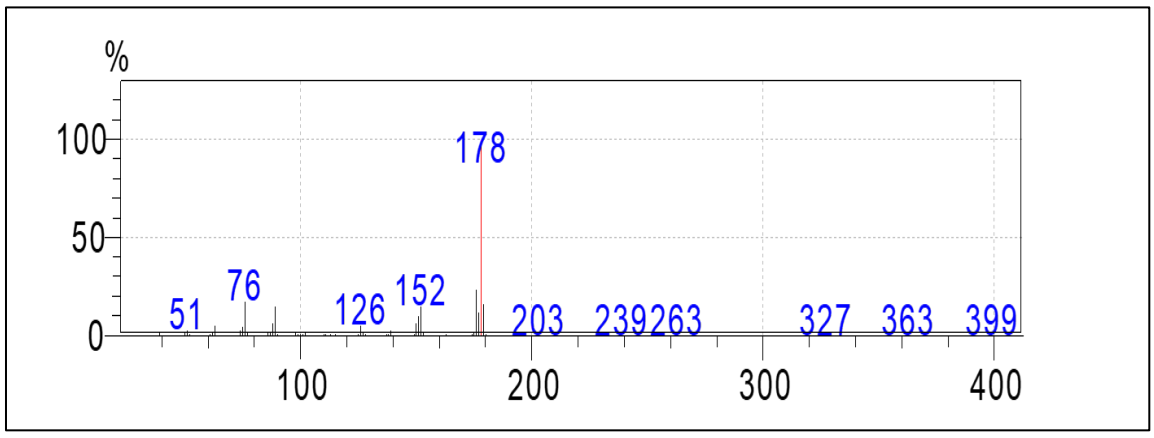

Figure A22 Experimental EI spectra for DPA NIST Ref:
https://webbook.nist.gov/cgi/cbook.cgi?ID=C501655&Mask=200#Mass-Spec

VITA

Andishaeh Patrick Dadgar

Candidate for the Degree of

Master of Science

Thesis: ENHANCED PLASMONIC PHOTOCATALYST FOR USE IN CROSS COUPLING REACTIONS

Major Field: Chemical Engineering

Career Focus

• Seeking full time employment in the chemical industry able to start summer of 2018

Education and Training

• Bachelor of Science in Chemical Engineering, Oklahoma State University May 2016
GPA: 3.966

• Masters of Science in Chemical Engineering, Oklahoma State University May 2018
GPA: 4.0

Presentations/Publications

• American Chemical Society National Conference Catalyst Division Spring 2016
  - Title: "Heterogeneous or Homogenous? A UV-Vis Approach"

• American Institute for Chemical Engineers National Conference Fall 2017
  - Title: "Plasmonic Catalyst as Efficient Catalyst for Cross Coupling Reactions"

• American Institute for Chemical Engineers National Conference Fall 2017
  - Title: "Design of Efficient Metal Nanocatalysts for Cross Coupling Reactions Using Finite Difference Time-Domain Simulations"

• American Institute for Chemical Engineers National Conference Fall 2017
  - Title: "Design of Efficient Metal Nanocatalysts for Continuous Synthesis of Drug Substances Via Cross Coupling Reactions".

• "Localized Surface Plasmon Resonance Spectroscopy as Platform for Characterization of Metal Nanoparticle Catalyzed Coupling Reactions" Submitted
JACS Summer 2018

• "Copper Only Catalyzed Sonogashira Coupling" In preparation Summer 2018